Received July 11, 2019, accepted July 18, 2019, date of publication July 23, 2019, date of current version August 12, 2019.

Digital Object Identifier 10.1109/ACCESS.2019.2930664

Security and Reliability Performance Analysis of Cooperative Multi-Relay Systems With Nonlinear Energy Harvesters and Hardware Impairments

XINGWANG LI[1], (Member, IEEE), MENGYAN HUANG[1], (Student Member, IEEE), CHANGSEN ZHANG[1], DAN DENG[2], (Member, IEEE), KHALED M. RABIE[3], (Member, IEEE), YUAN DING[4], AND JIANHE DU[5]

[1]School of Physics and Electronic Information Engineering, Henan Polytechnic University, Jiaozuo 454000, China
[2]Guangzhou Panyu Polytechnic, Guangzhou 511483, China
[3]Faculty of Science and Engineering, Manchester Metropolitan University, Manchester M1 5GD, U.K.
[4]Institute of Sensors, Signals, and Systems, Heriot-Watt University, Edinburgh EH14 4AS, U.K.
[5]School of Information and Communication Engineering, Communication University of China, Beijing 100024, China

Corresponding author: Changsen Zhang (zhangchangsen@hpu.edu.cn)

This work was supported in part by the Henan Scientific and Technological Research Project under Grant 182102210307, in part by the Doctoral Scientific Funds of Henan Polytechnic University under Grant B2016-34, in part by the Fundamental Research Funds for the Universities of Henan Province under Grant NSFRF180309, in part by the Outstanding Youth Science Foundation of Henan Polytechnic University under Grant J2019-4, in part by the National Natural Science Foundation of China under Grant 61601414, in part by the Fundamental Research Funds for the Central Universities under Grants 010403302/CUC18A007-2 and Grant 3132018XNG1808, in part by the Natural Science Foundation of Guangdong Province under Grant 2018A030313736, in part by the Scientific Research Project of Education Department of Guangdong, China, under Grant 2017GKTSCX045, in part by the Science and Technology Program of Guangzhou, China, under Grant 201707010389, and in part by the Key Scientific Research Projects of Higher Education Institutions in Henan Province under Grant 20A510007.

ABSTRACT In this paper, we investigate the reliability and security performance of cooperative multi-relay systems, where both source and relay nodes are energy-constrained nonlinear energy harvesters, scavenging energy from a power beacon nearby. Our analysis is based on practical model since residual hardware impairments (RHIs) and channel estimation errors (CEEs) are considered. Aiming at improving the system efficiency, three representative relay selection strategies are considered: 1) random relay selection (RRS); 2) suboptimal relay selection (SRS); and 3) optimal relay selection (ORS). To characterize the security performance of the considered strategies, we derive closed-form analytical expressions of the reliability and security in terms of outage probability (OP) and intercept probability (IP). We further discuss the asymptotic expressions and scaling laws of OP with the number of relays. The IP is analyzed for non-colluding and colluding scenarios. The numerical results illustrate that: 1) There is a tradeoff between reliability and security, that is when the outage constraint is relaxed, the IP can be enhanced, and vice versa; ii) The outage performance of the ORS and SRS schemes outperform RRS, indicating that relay selection can enhance reliability performance; iii) There are error floors for the OP due to the CEEs; iv) Colluding eavesdroppers can enhance eavesdropping attacks by sharing their intercepted information; and v) Although RHIs and CEEs have deleterious effects on the OP, they can protect the information transmission against eavesdropping attacks.

INDEX TERMS Physical layer security, hardware impairments, nonlinear energy harvesters, relay selection, reliability-security tradeoff.

I. INTRODUCTION

Cooperative wireless communication networks (WCNs) have been widely used in military, agricultural and industrial fields, etc [1]–[6]. Authors in [1] introduced the principles of cooperative WCNs and discussed some practical applications in wireless environments, i.e., surveillance video transmission, mine monitoring, wireless telephone applications *et al.* The authors in [2] studied the secure performance of a direct-sequence code-division multiple access (DS-CDMA)

The associate editor coordinating the review of this manuscript and approving it for publication was Prabhat Kumar Upadhyay.

systems and derived the expressions of bit error probability (BEP), outage probability (OP) and channel capacity (CC). The authors obtained the approximate OP and average symbol error rate (SER) for cooperative DS-CDMA systems over asymmetric fading channels [3]. In [4], the authors studied the outage performance for the classical spatial modulation (SM) system and extended the results to the cooperative scenarios under fixed, selective and incremental relaying techniques. However, due to the broadcast nature of radiated electromagnetic waves, the WCNs are vulnerable to intrusion threats of eavesdroppers attempting to overhear the legitimate communication. Although encryption techniques can solve this problem by using various mathematic based algorithms, it will incur extra overhead and complexity [7]. As an alternative security technology, physical layer security (PLS) has been proposed as an efficient and effective way to ensure the security and reliability of WCNs [8]. Different from the traditional key-based cryptographic techniques, PLS exploits the characteristics of physical wireless channels to guarantee secure communication between source to its intended destination, avoiding complex encryption/decryption algorithms. However, when the quality of the main link between source and destination is worse than that of the wiretap link between source and eavesdropper, the secure communication may not be obtained. To solve this problem, multi-antenna technique has been introduced to strength the PLS of WCNs [9]–[12]. In [9], the authors characterized the secrecy capacity of the single input multiple output (SIMO) channel under Gaussian noise and studied the impact of slow fading on the secrecy capacity of the systems. The authors of [10] considered that the transmitter communicates with the receiver in the presence of the eavesdropper under the condition of Gaussian multiple input single output (MISO) channel and the optimal beamforming transmission strategy was designed according to the input covariance matrix under different channel fading. In [11], the authors studied the PLS of multiple input multiple output (MIMO) radio frequency identification (RFID) systems in view of the resource limitation of backscatter systems, and proposed a noise injection precoding strategy to address the maximum secrecy rate (MSR) problem. Besides, the authors of [12] analyzed the PLS in millimeter-wave (mmWave) communications over fluctuating two-ray (FTR) fading channels, and derived the expressions for the average secrecy capacity (ASC), secrecy outage probability (SOP) and the probability of strictly positive secrecy capacity (SPSC).

Cooperative communication has been identified as a promising technology for the future mobile communication because of extending network coverage and reducing transmit power [13]–[15]. To further improve the networks performance, multi-antenna technology can be introduced into cooperative communication [16]–[20]. A review on state-of-the-art PLS aspects of cooperative multi-relay networks was presented in [16]. In [17], a destination-assisted jamming and beamforming scheme of cooperative amplify-and-forward (AF) relaying systems was proposed, in which the optimal beamformer weights and power allocation were obtained by solving linear programming problem. Moreover, [18] proposed a cooperative scheme by combining transmit antenna selection (TAS) and space shift keying (SSK) for MIMO system. In [19], the outage performance of AF DS-CDMA systems with best selection over $\alpha-\eta-\mu$ fading channels was analyzed and the expressions of OP and cumulative distribution function (CDF) were derived. The authors in [20] proposed an AF MIMO relaying scheme and derived the error probability for the considered cooperative systems. However, deploying multiple relays may incur extra inter-relay interference and make it more vulnerable to the potential eavesdroppers. To enhance the security, relay selection (RS) has been recognized as an effective solution [21]–[26]. The authors of [21] investigated the PLS in cooperative wireless networks based on optimal RS (ORS) by considering AF and DF protocols, and the diversity order and intercept probability (IP) were derived. In [22], the ORS and suboptimal RS (SRS) schemes based on global channel state information (CSI) and only source-destination (SD) pairs CSI were proposed, in order to evaluate the performance of system PLS under this scheme, the accurate SOP of SRS scheme under two residual self-interference models was obtained. [23] investigated the PLS of maximal ratio combining (MRC) strategy in wiretap two-wave based on diffuse power fading channels and derived the expressions for the ASC based on two practical scenarios. Furthermore, the authors in [24] proposed an efficient mobile RS scheme for the original combinatorial optimization based on the emerging cooperative non-orthogonal multiple access (NOMA) systems. In [25], the joint relay station, related sub-channel and power allocation problem was studied underlying cellular networks for relay-aided device-to-device (D2D) communications. In [26], the authors aimed to optimize system throughput of the hybrid system via joint consideration of mode selection and resource allocation, which includes admission control, power control, channel assignment and RS. Although the performance of WCNs can be improved through the proper RS and eavesdropper connection, in the typical communication scheme, the performance of wireless nodes is constrained by the power shortages due to huge path loss [27].

Communication systems are generally power limited, especially for the battery powered devices. To solve this problem, it is encouraged to adopt wireless power compensating techniques such as energy harvesting (EH) [28]–[30]. For EH, the energy can be harvested from wind, solar, magnetic induction, etc. Among the various renewable EH, radio frequency (RF)-enabled simultaneous wireless information and power transfer (SWIPT) has been recognized as an effective way to prolong the battery life of wireless devices [31]–[36]. In general, there are two typical protocols for SWIPT systems: time-switching (TS) protocol and power-splitting (PS) protocol [37]–[41]. In [37], the authors carried out the bit error performance of a power-based cooperative AF relaying system, where PS, TS and ideal operational protocols are taken into account. In [38], the authors have proposed TS and PS protocols under the communication system to enable EH and information processing at the relay. To improve the security for the source-to-destination link of TS based DF relay networks, a FD jammer protocol and its half-duplex version were proposed [39]. Considering multi-antenna systems, a joint beamforming and time switching scheme was designed to maximize the system secrecy rate of wireless power FD relay networks [40]. Inspired by NOMA systems, outage performance analysis of TS based SWIPT cooperative NOMA networks over Weibull fading channels was carried out [6]. In [41], the authors studied a multi-relay selection scheme of EH-based bidirectional relay system, where the relay node adopts the PS protocol. The authors investigated the performance for SWIPT cooperative systems in presence of a direct link from source to destination in [42] and [43].

The aforementioned research works are based on ideal hardware components and ideal CSI, which is not realistic in practical communication systems. In practice, the transmitters and receivers of communication systems may suffer from multiple types of hardware impairments (HIs), such as high-power amplifier non-linearity, phase noise, in-phase/quadrature-phase (I/Q) imbalance and etc [44], [45]. These impairments can generally be eliminated through some compensation algorithms. However, due to the internal characteristics of RF components, the above impairments cannot be completely removed [14], [46], [47]. Furthermore, due to the presence of channel estimation errors (CEEs), imperfect channel state information (ICSI) may occur. Therefore, it is of great practical significance to consider the impact of residual hardware impairments (RHIs) on the security performance of cooperative relay communication networks.

A. MOTIVATION AND CONTRIBUTIONS

Motivated by the above observations, we investigate the secure performance of cooperative multi-relay systems with nonlinear energy harvesters and ICSI, where RHIs at all nodes are taken into account. Considering these imperfections, three RS strategies are proposed, namely RRS, SRS and ORS. Specifically, we focus on the security and reliability in terms of OP and IP. We assume that source and relay nodes equip nonlinear energy harvesters with different saturation thresholds to collect energy from a nearby power beacon. The contributions of this paper are summarized as below:

- Considering RHIs, ICSI and non-linear energy harvesters, we propose three RS strategies, namely RRS, ORS and SRS. RRS is provided as a benchmark for the purpose of comparison, in which the relay is selected randomly. In ORS, the optimal relay is selected according the link quality of both source-to-relay and relay-to-destination. To achieve the tradeoff between performance and complexity, SRS scheme is proposed, that is, an optimal relay is selected between $S \to R_m$ or $R_m \to D$ according to the link quality.
- We evaluate the reliability and security performance of cooperative multi-relay systems by deriving the analytical expressions for OP and IP. For eavesdroppers, both non-colluding and colluding eavesdropping scenarios are considered.
- We further analyze the asymptotic behavior of the proposed strategies by studying the scaling laws as the number of relays M approaches infinity for the OP, which provides some useful insights. The results show that RRS is irrelevant to the number of relay, while SRS and ORS can improve the secure performance.

B. ORGANIZATION

The rest of the paper is organized as follows: In Section II, we present the impaired cooperative multi-relay system model with non-linear energy harvesters and ICSI. In Section III, the analytical closed-form expressions for the OP and IP of the proposed schemes are derived and the scaling laws of OP with the number of relay are analyzed. In Section IV, some numerical results and key findings are provided and discussed. Section V summarizes the paper.

C. NOTATION

We use $\mathcal{CN}\left(\mu, \sigma^2\right)$ to denote the complex Gaussian random variable with mean μ and variance σ^2. Notations $|\cdot|$ and $E\{\cdot\}$ represent the absolute value and expected operators, respectively. $f_X(\cdot)$ and $F_X(\cdot)$ are the probability density function (PDF) and the CDF of random variable X, respectively. The vth-order modified Bessel function of the second kind is denoted by $K_v(\cdot)$ and $\Pr\{\cdot\}$ is the probability. Finally, the $\log(\cdot)$ is the logarithm.

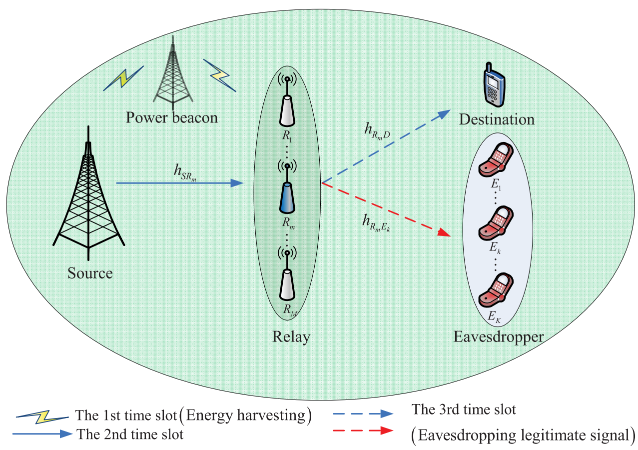

FIGURE 1. System model of power beacon-assisted secure network.

II. SYSTEM MODEL

As illustrated in Fig. 1, we consider a power beacon assisted cooperative multi-relay system, which consists of one power beacon B, one source S, M relays R_m, $m \in \{1, 2, \cdots, M\}$ and K eavesdroppers E_k, $k \in \{1, 2, \cdots, K\}$. Aiming at improving the secure performance, the optimal relay is selected among M relays by using RRS, SRS and ORS. Source and all relays are energy-constrained which can harvest energy from a nearby power beacon according TS protocol. It is assume that all nodes equip a single antenna. We further assume that the direct links both $S \to D$ and $S \to E_k$ are absent due to heavy shadow fading [28], [29].[1]

In practice, it is difficult to obtain perfect CSI due to some CEEs. Some channel estimation algorithms are necessary to obtain CSI. To this end, linear minimum mean square error (MMSE) is adopted. Thus, channel can be modeled as

$$h_i = \hat{h}_i + e_i, \tag{1}$$

where $e_i, i \in \{SR_m, R_mD, R_mE_k\}$ is the CEE with $e_i \sim \mathcal{CN}\left(0, \sigma_{e_i}^2\right)$, $\hat{h}_i$ is the estimated channel of real channel h_i.

In this paper, we assume that all links experience Rayleigh fading and path loss [13]. The entire communication process is divided into three time slots: 1) S and relays collect energy from B; 2) S transmits own signal to R_m; 3) R_m decodes and forwards the signals to D and E.

The first time slot: In the first phase, S and R_m harvest energy from B. The harvested energy at S is

$$E_S = \zeta_1 P_B |h_{BS}|^2 \alpha T, \tag{2}$$

where h_{BS} is the transmission channel from B to S; ζ_1 $(0 \leq \zeta_1 \leq 1)$ is the energy conversion efficiency at S; α $(0 < \alpha < 1)$ is the time allocation factor; T is the block transmission duration; P_B is the transmission power at B; E_S is used to transmit information in the second time slot. In the presence of the nonlinear energy harvester, the output power, P_S can be expressed as [49]

$$P_S = \begin{cases} \dfrac{2\alpha\zeta_1 P_B}{1-\alpha}|h_{BS}|^2, & \textit{if } P_B|h_{BS}|^2 \leq \Gamma_1 \\ \dfrac{2\alpha\zeta_1}{1-\alpha}\Gamma_1, & \textit{if } P_B|h_{BS}|^2 > \Gamma_1 \end{cases} \tag{3}$$

where Γ_1 is the saturated threshold at S of the harvester.

Similarly, the harvested energy at R_m is

$$E_{R_m} = \zeta_2 P_B \left|h_{BR_m}\right|^2 \alpha T, \tag{4}$$

where h_{BR_m} is the transmission channel from B to R_m; ζ_2 $(0 \leq \zeta_2 \leq 1)$ is the energy conversion efficiency at R_m. Under the condition of non-linear energy harvesters, the output power at the R_m, P_{R_m}, is

$$P_{R_m} = \begin{cases} \dfrac{2\alpha\zeta_2 P_B}{1-\alpha}\left|h_{BR_m}\right|^2, & \textit{if } P_B\left|h_{BR_m}\right|^2 \leq \Gamma_2 \\ \dfrac{2\alpha\zeta_2}{1-\alpha}\Gamma_2, & \textit{if } P_B\left|h_{BR_m}\right|^2 > \Gamma_2, \end{cases} \tag{5}$$

where Γ_2 is the saturated threshold at R_m of the harvester.

The second time slot: In this phase, S transmits signal x_{SR_m} to R_m with $E\left\{\left|x_{SR_m}\right|^2\right\} = 1$. Considering the RHIs and ICSI [44]–[46], the received signal at R_m can be expressed as

$$y_{SR_m} = \left(\hat{h}_{SR_m} + e_{SR_m}\right)\left(\sqrt{P_S}x_{SR_m} + \eta_{t,SR_m}\right) + \eta_{r,SR_m} + \upsilon_{SR_m}, \tag{6}$$

where $\hat{h}_{SR_m}$ is the estimated channel between S and R_m; η_{t,SR_m} and η_{r,SR_m} are the distortion noises of RHIs at transmitter and receiver, respectively; $\upsilon_{SR_m} \sim \mathcal{CN}\left(0, N_{SR_m}\right)$ is the complex additive white Gaussian noise (AWGN). As stated in [46], the distortion noises are defined as

$$\eta_{t,SR_m} \sim CN\left(0, \kappa_{t,SR_m}^2 P_S\right), \quad \eta_{r,SR_m} \sim CN\left(0, \kappa_{r,SR_m}^2 P_S \left|h_{SR_m}\right|^2\right), \tag{7}$$

the effective distortion noise can be seen as two independent jointly Gaussian variable η_{t,SR_m} and $\eta_{r,SR_m}/h_{SR_m}$ that are multiplied with the fading channel h_{SR_m}. For a given channel realization h_{SR_m}, the aggregated distortion seen at the receiver has power

$$\begin{aligned} E_{\eta_{t,SR_m},\eta_{r,SR_m}}&\left\{\left|h_{SR_m}\eta_{t,SR_m} + \eta_{r,SR_m}\right|^2\right\} \\ &= P_S\left|h_{SR_m}\right|^2\left(\kappa_{t,SR_m}^2 + \kappa_{r,SR_m}^2\right) \\ &= P_S\left|\hat{h}_{SR_m} + e_{SR_m}\right|^2\left(\kappa_{t,SR_m}^2 + \kappa_{r,SR_m}^2\right), \end{aligned} \tag{8}$$

we can observe that it only depends on the average signal power P_S and the instantaneous channel gain $\left|h_{SR_m}\right|^2$. We have the definition that $\kappa_{SR_m} = \sqrt{\kappa_{t,SR_m}^2 + \kappa_{r,SR_m}^2}$. Thus, the received signal at R_m can be rewritten as:

$$y_{SR_m} = \left(\hat{h}_{SR_m} + e_{SR_m}\right)\left(\sqrt{P_S}x_{SR_m} + \eta_{SR_m}\right) + \upsilon_{SR_m}, \tag{9}$$

where $\eta_{SR_m} \sim \mathcal{CN}\left(0, \kappa_{SR_m}^2 P_S\right)$ is the aggregate distortion noise at the transmitter and receiver.

The third time slot: The signals x_{R_mD} and $x_{R_mE_k}$ are transmitted from R_m to D and from R_m to E_k, respectively. Similarly, the received signals at D and E_k can be expressed as

$$y_{R_mD} = \left(\hat{h}_{R_mD} + e_{R_mD}\right)\left(\sqrt{P_{R_m}}x_{R_mD} + \eta_{R_mD}\right) + \upsilon_{R_mD}, \tag{10}$$

$$y_{R_mE_k} = \left(\hat{h}_{R_mE_k} + e_{R_mE_k}\right)\left(\sqrt{P_{R_m}}x_{R_mE_k} + \eta_{R_mE_k}\right) + \upsilon_{R_mE_k}, \tag{11}$$

where $\eta_{R_mD} \sim \mathcal{CN}\left(0, \kappa_{R_mD}^2 P_{R_m}\right)$ and $\eta_{R_mE_k} \sim \mathcal{CN}\left(0, \kappa_{R_mE_k}^2 P_{R_m}\right)$ are the aggregated distortion noises at the transmitter and receiver, such that $\kappa_{R_mD} \triangleq \sqrt{\kappa_{t,R_mD}^2 + \kappa_{r,R_mD}^2}$ and $\kappa_{R_mE_k} \triangleq \sqrt{\kappa_{t,R_mE_k}^2 + \kappa_{r,R_mE_k}^2}$.

Therefore, the received signal-to-interference-plus-noise ratios (SINRs) at R_m, D and E_k can be finally obtained as

$$\gamma_{SR_m} = \frac{\rho_{SR_m}\left|\hat{h}_{SR_m}\right|^2}{\rho_{SR_m}\left|\hat{h}_{SR_m}\right|^2\kappa_{SR_m}^2 + \rho_{SR_m}\sigma_{e_{SR_m}}^2\left(1+\kappa_{SR_m}^2\right) + 1}, \tag{12}$$

$$\gamma_{R_mD} = \frac{\rho_{R_mD}\left|\hat{h}_{R_mD}\right|^2}{\rho_{R_mD}\left|\hat{h}_{R_mD}\right|^2\kappa_{R_mD}^2 + \rho_{R_mD}\sigma_{e_{R_mD}}^2\left(1+\kappa_{R_mD}^2\right) + 1}, \tag{13}$$

$$\gamma_{R_mE_k} = \frac{\rho_{R_mE_k}\left|\hat{h}_{R_mE_k}\right|^2}{\rho_{R_mE_k}\left|\hat{h}_{R_mE_k}\right|^2\kappa_{R_mE_k}^2 + \rho_{R_mE_k}\sigma_{e_{R_mE_k}}^2\left(1+\kappa_{R_mE_k}^2\right) + 1}, \tag{14}$$

[1] In some scenarios, eavesdroppers may intercept information from the source and relay, simultaneously. We will set aside this assumption in our future work.

where $\rho_{SR_m} = P_S / N_{SR_m}$, $\rho_{R_mD} = P_{R_m} / N_{R_mD}$ and $\rho_{R_mE_k} = P_{R_m} / N_{R_mE_k}$.

According to the Shannon's information, we can obtain the channel capacities of $S \to R_m$, $R_m \to D$ and $R_m \to E_k$ as [51]

$$C_{SR_m} = \frac{1-\alpha}{2} \log_2 \left(1 + \gamma_{SR_m}\right), \tag{15}$$

$$C_{R_mD} = \frac{1-\alpha}{2} \log_2 \left(1 + \gamma_{R_mD}\right), \tag{16}$$

$$C_{R_mE_k} = \frac{1-\alpha}{2} \log_2 \left(1 + \gamma_{R_mE_k}\right), \tag{17}$$

where the factor $\frac{1-\alpha}{2}$ can be explained by the fact that the relays operate in half-duplex mode and requires two time slots to complete the transmission of S to D through R_m.

According to DF protocol, the effective end-to-end capacity of R_m and D can be expressed as

$$C_{R_m} = \min \left(C_{SR_m}, C_{R_mD}\right). \tag{18}$$

III. RELIABILITY AND SECURITY PERFORMANCE ANALYSIS

To evaluate the reliability and security of the hardware impaired multi-relay network powered through EH, we study the OP and IP performance of RRS, SRS, ORS in the networks. Moreover, the scaling-law for the OP is discussed when the number of relays approaches infinity. For security, both non-colluding and colluding eavesdropping scenarios are considered.[2]

A. OUTAGE PROBABILITY ANALYSIS

In this subsection, we study the OP of the multi-relay networks in presence of RHIs and ICSI for the considered RS strategies.

Outage Probability: Referring to [13], OP is defined as the probability that the effective channel capacity is below a threshold C_{th} and it can be expressed as

$$P_{out} \triangleq \Pr\left\{C_R < C_{th}\right\}, \tag{19}$$

where C_R is the effective end-to-end channel capacity.

1) RRS

For RRS scheme, a relay is randomly selected among M relays of $S \to R_m$, which formulated as

$$C_{R_m} = \min \left(C_{SR_m}, C_{R_mD}\right) \tag{20}$$

From (19) and (20), the following theorem is provided about OP for the RRS scheme.

Theorem 1: The exact analytical expressions for OP of RRS scheme under non-ideal and ideal conditions are provided in (21) and (22), as shown at the bottom of this page.[3]

For $\varepsilon < 1 / \max\left(\kappa_{SR_m}^2, \kappa_{R_mD}^2\right)$, otherwise OP is equal to 1.

where $\varepsilon = 2^{\frac{2C_{th}}{1-\alpha}} - 1$, $A_1 = \frac{2\alpha\zeta_1}{1-\alpha}$, $C_1 = A_1 P_B \left(1 - \varepsilon\kappa_{SR_m}^2\right)$, $C_2 = \varepsilon A_1 P_B \sigma_{e_{SR_m}}^2 \left(1 + \kappa_{SR_m}^2\right)$, $E_1 = \frac{\Gamma_1}{P_B}$, $T_1 = \frac{\varepsilon N_{SR_m}}{C_1 E_1} + \frac{C_2}{C_1}$, $u_1 = \frac{\varepsilon N_{SR_m}}{E_1}$, $\beta_1 = \lambda_{BS}\varepsilon N_{SR_m}$, $\gamma_1 = \frac{\lambda_{SR_m}}{C_1}$,

[2]Here, bit error rate (BER) is also a measurement standard that can reflect the system performance [37], [51], and we will further expand the research in the future study.

[3]Non-ideal conditions mean that the system has RHIs or CEEs. The ideal conditions are that the RHIs parameter $\kappa_i = 0$ and CEEs parameter $\sigma_{e_i}^2 = 0$.

$$\begin{aligned} P_{out}^{RRS,ni} = 1 - &\left[\frac{2\lambda_{SR_m}}{C_1} e^{-\frac{\lambda_{SR_m} C_2}{C_1}} \sqrt{\frac{\beta_1}{\gamma_1}} K_1\left(2\sqrt{\beta_1\gamma_1}\right) + e^{-\lambda_{BS}E_1}\left(e^{-\lambda_{SR_m}\Theta_1} - e^{-\lambda_{SR_m}T_1}\right) - \frac{\pi u_1 \lambda_{SR_m}}{2Y_1 C_1} e^{-\frac{\lambda_{SR_m}C_2}{C_1}} \sum_{l_1=0}^{Y_1} \sqrt{1-\delta_{l_1}^2} \right. \\ &\left. \times e^{-\frac{2\beta_1}{u_1\left(\delta_{l_1}+1\right)} - \frac{u_1\gamma_1\left(\delta_{l_1}+1\right)}{2}} \right] \left[\frac{2\lambda_{R_mD}}{C_3} e^{-\frac{\lambda_{R_mD}C_4}{C_3}} \sqrt{\frac{\beta_2}{\gamma_2}} K_1\left(2\sqrt{\beta_2\gamma_2}\right) + e^{-\lambda_{BR_m}E_2}\left(e^{-\lambda_{R_mD}\Theta_2} - e^{-\lambda_{R_mD}T_3}\right) \right. \\ &\left. - \frac{\pi u_2 \lambda_{R_mD}}{2Y_2C_3} \sum_{l_2=0}^{Y_2} \sqrt{1-\delta_{l_2}^2} \times e^{-\frac{\lambda_{R_mD}C_4}{C_3} - \frac{2\beta_2}{u_2\left(\delta_{l_2}+1\right)} - \frac{u_2\gamma_2\left(\delta_{l_2}+1\right)}{2}} \right] \end{aligned} \tag{21}$$

$$\begin{aligned} P_{out}^{RRS,id} = 1 - &\left[\frac{2\lambda_{SR_m}}{C_{12}} \sqrt{\frac{\beta_1}{\gamma_{12}}} K_1\left(2\sqrt{\beta_1\gamma_{12}}\right) + e^{-\lambda_{BS}E_1}\left(e^{-\lambda_{SR_m}\Theta_{12}} - e^{-\lambda_{SR_m}T_{12}}\right) - \frac{\pi u_1 \lambda_{SR_m}}{2Y_1 C_{12}} \sum_{l_1=0}^{Y_1} \sqrt{1-\delta_{l_1}^2} \right. \\ &\left. \times e^{-\frac{2\beta_1}{u_1\left(\delta_{l_1}+1\right)} - \frac{u_1\gamma_{12}\left(\delta_{l_1}+1\right)}{2}} \right] \left[\frac{2\lambda_{R_mD}}{C_{32}} \sqrt{\frac{\beta_2}{\gamma_{22}}} K_1\left(2\sqrt{\beta_2\gamma_{22}}\right) + e^{-\lambda_{BR_m}E_2}\left(e^{-\lambda_{R_mD}\Theta_{22}} - e^{-\lambda_{R_mD}T_{32}}\right) \right. \\ &\left. - \frac{\pi u_2 \lambda_{R_mD}}{2Y_2C_{32}} \sum_{l_2=0}^{Y_2} \sqrt{1-\delta_{l_2}^2}\, e^{-\frac{2\beta_2}{u_2\left(\delta_{l_2}+1\right)} - \frac{u_2\gamma_{22}\left(\delta_{l_2}+1\right)}{2}} \right] \end{aligned} \tag{22}$$

$\delta_{l_1} = \cos\left[\frac{(2l_1-1)\pi}{2Y_1}\right]$, $\Theta_1 = \frac{\varepsilon A_1\Gamma_1\sigma_{e_{SR_m}}^2\left(1+\kappa_{SR_m}^2\right)+\varepsilon N_{SR_m}}{A_1\Gamma_1\left(1-\varepsilon\kappa_{SR_m}^2\right)}$, $A_2 = \frac{2\alpha\zeta_2}{1-\alpha}$, $C_3 = A_2P_B\left(1-\varepsilon\kappa_{R_mD}^2\right)$, $C_4 = \varepsilon A_2P_B\sigma_{e_{R_mD}}^2\left(1+\kappa_{R_mD}^2\right)$, $E_2 = \frac{\Gamma_2}{P_B}$, $T_3 = \frac{\varepsilon N_{R_mD}}{C_3E_2}+\frac{C_4}{C_3}$, $u_2 = \frac{\varepsilon N_{R_mD}}{E_2}$, $\beta_2 = \lambda_{BR_m}\varepsilon N_{R_mD}$, $\gamma_2 = \frac{\lambda_{R_mD}}{C_3}$, $\delta_{l_2} = \cos\left[\frac{(2l_2-1)\pi}{2Y_2}\right]$, $\Theta_2 = \frac{\varepsilon A_2\Gamma_2\sigma_{e_{R_mD}}^2\left(1+\kappa_{R_mD}^2\right)+\varepsilon N_{R_mD}}{A_2\Gamma_2\left(1-\varepsilon\kappa_{R_mD}^2\right)}$, $C_{12} = A_1P_B$, $T_{12} = \frac{\varepsilon N_{SR_m}}{C_{12}E_1}$, $\Theta_{12} = \frac{\varepsilon N_{SR_m}}{A_1\Gamma_1}$, $\gamma_{12} = \frac{\lambda_{SR_m}}{C_{12}}$, $C_{32} = A_2P_B$, $T_{32} = \frac{\varepsilon N_{R_mD}}{C_{32}E_2}$, $\Theta_{22} = \frac{\varepsilon N_{R_mD}}{A_2\Gamma_2}$ and $\gamma_{22} = \frac{\lambda_{R_mD}}{C_{32}}$.

Proof: See Appendix A. □

In order to obtain useful insights, the following corollary provides the asymptotic analysis for OP of RRS scheme under non-ideal conditions in the high SNR region.

Corollary 1: The asymptotic analysis for OP of RRS scheme under non-ideal conditions is given by

$$P_{out}^{RRS,\infty} = 1 - e^{-\lambda_{SR_m}\Theta_{A_1}-\lambda_{R_mD}\Theta_{A_2}}, \tag{23}$$

where $\Theta_{A_1} = \frac{\varepsilon\sigma_{e_{SR_m}}^2\left(1+\kappa_{SR_m}^2\right)}{1-\varepsilon\kappa_{SR_m}^2}$ and $\Theta_{A_2} = \frac{\varepsilon\sigma_{e_{R_mD}}^2\left(1+\kappa_{R_mD}^2\right)}{1-\varepsilon\kappa_{R_mD}^2}$.

Proof: According to (15), (16) and (17), the channel capacity of $S \to R_m$, $R_m \to D$ and $R_m \to E_k$ in the high SNR region can be expressed uniformly as

$$C_i^{\infty} = \frac{1-\alpha}{2}\log_2\left(1+\frac{\left|\hat{h}_i\right|^2}{\left|\hat{h}_i\right|^2\kappa_i^2+\sigma_{e_i}^2\left(1+\kappa_i^2\right)}\right). \tag{24}$$

From the definition of OP, the following expression can be obtained as

$$\begin{aligned} P_{out}^{RRS,\infty} &= \Pr\left\{\min\left(C_{SR_m}^{\infty}, C_{R_mD}^{\infty}\right) < C_{th}\right\} \\ &= 1-\Pr\left\{C_{SR_m}^{\infty} > C_{th}\right\}\Pr\left\{C_{R_mD}^{\infty} > C_{th}\right\}. \end{aligned} \tag{25}$$

By utilizing the similar methodology of Appendix A, we can obtain the result of (23). □

To obtain more insights, the asymptotic analysis for RRS scheme is studied as the number of relays approaches infinity. The scaling law with respect to M for the OP is defined in [55]

$$d_j^{RRS} = \lim_{M\to\infty}\frac{\log\left(P_{out}^{RRS,j}\right)}{M}, \quad j \in \{ni, id\}, \tag{26}$$

where M is the number of relays, P_{out}^{RRS} is the OP for RRS scheme.

Corollary 2: The scaling laws for the RRS scheme under the non-ideal and ideal conditions are given by

- *Non-ideal conditions*

$$d_{ni}^{RRS} = \lim_{M\to\infty}\frac{\log\left(P_{out}^{RRS,ni}\right)}{M} = 0, \tag{27}$$

- *Ideal conditions*

$$d_{id}^{RRS} = \lim_{M\to\infty}\frac{\log\left(P_{out}^{RRS,id}\right)}{M} = 0, \tag{28}$$

Proof: The proof follows by combining **Theorem 1** with (26) and taking M to infinity. □

*Remark 1: From **Theorem 1** and **Corollary 2**, we have some insights on the derived results. For imperfect RFs, there is an upper bound for the effective SINR at high SNRs for $\varepsilon < 1\big/\max\left(\kappa_{SR_m}^2, \kappa_{R_mD}^2\right)$, which results in an error floor for the OP. In addition, we can observe that scaling laws approach to zero as the number of relays grows into infinity for perfect and imperfect RFs. This means that for RRS, the reliability performance is irrelative to the number of relays, that is, we can not improve OP performance by increasing the number of relays.*

2) SRS

For SRS scheme, we choose a relay to maximize the channel capacity of $S \to R_m$,[4] which are formulated as

$$b = \arg\max_{m=1,2,\cdots,M} C_{SR_m}, \tag{29}$$

$$C_{R_b} = \min\left(C_{SR_b}, C_{R_bD}\right). \tag{30}$$

Utilizing the above definitions, the OP for SRS scheme is presented in the following theorem.

Theorem 2: The exact analytical expressions for OP of SRS scheme under non-ideal and ideal conditions are provided in (31) and (32), as shown at the top of the next page,

where $\omega = M\sum_{s=0}^{M-1}\binom{M-1}{s}(-1)^s$, $C_5 = A_1P_B\left(1-\varepsilon\kappa_{SR_b}^2\right)$, $C_6 = \varepsilon A_1P_B\sigma_{e_{SR_b}}^2\left(1+\kappa_{SR_b}^2\right)$, $T_5 = \frac{\varepsilon N_{SR_b}}{C_5E_1}+\frac{C_6}{C_5}$, $u_3 = \frac{\varepsilon N_{SR_b}}{E_1}$, $\beta_3 = \lambda_{BS}\varepsilon N_{SR_b}$, $\gamma_3 = \frac{\lambda_{SR_b}(s+1)}{C_5}$, $\delta_{l_3} = \cos\left[\frac{(2l_3-1)\pi}{2Y_3}\right]$, $\Theta_3 = \frac{\varepsilon A_1\Gamma_1\sigma_{e_{SR_b}}^2\left(1+\kappa_{SR_b}^2\right)+\varepsilon N_{SR_b}}{A_1\Gamma_1\left(1-\varepsilon\kappa_{SR_b}^2\right)}$, $C_7 = A_2P_B\left(1-\varepsilon\kappa_{R_bD}^2\right)$, $C_8 = \varepsilon A_2P_B\sigma_{e_{R_bD}}^2\left(1+\kappa_{R_bD}^2\right)$, $T_7 = \frac{\varepsilon N_{R_bD}}{C_7E_2}+\frac{C_8}{C_7}$, $u_4 = \frac{\varepsilon N_{R_bD}}{E_2}$, $\beta_4 = \lambda_{BR_b}\varepsilon N_{R_bD}$, $\gamma_4 = \frac{\lambda_{R_bD}}{C_7}$, $\delta_{l_4} = \cos\left[\frac{(2l_4-1)\pi}{2Y_4}\right]$, $\Theta_4 = \frac{\varepsilon A_2\Gamma_2\sigma_{e_{R_bD}}^2\left(1+\kappa_{R_bD}^2\right)+\varepsilon N_{R_bD}}{A_2\Gamma_2\left(1-\varepsilon\kappa_{R_bD}^2\right)}$, $C_{52} = A_1P_B$, $T_{52} = \frac{\varepsilon N_{SR_b}}{C_{52}E_1}$, $\Theta_{32} = \frac{\varepsilon N_{SR_b}}{A_1\Gamma_1}$, $\gamma_{32} = \frac{\lambda_{SR_b}(s+1)}{C_{52}}$, $C_{72} = A_2P_B$, $T_{72} = \frac{\varepsilon N_{R_bD}}{C_{72}E_2}$, $\Theta_{42} = \frac{\varepsilon N_{R_bD}}{A_2\Gamma_2}$ and $\gamma_{42} = \frac{\lambda_{R_bD}}{C_{72}}$.

Proof: See Appendix B. □

Similar to **Corollary 1**, the following asymptotic expressions for SRS scheme can be obtained.

Corollary 3: The asymptotic analysis for OP of SRS scheme under non-ideal conditions is given by

$$P_{out}^{SRS,\infty} = 1-\left[1-\left(1-e^{-\lambda_{SR_b}\Theta_{A_3}}\right)^M\right]e^{-\lambda_{R_bD}\Theta_{A_4}}, \tag{33}$$

where $\Theta_{A_3} = \frac{\varepsilon\sigma_{e_{SR_b}}^2\left(1+\kappa_{SR_b}^2\right)}{1-\varepsilon\kappa_{SR_b}^2}$ and $\Theta_{A_4} = \frac{\varepsilon\sigma_{e_{R_bD}}^2\left(1+\kappa_{R_bD}^2\right)}{1-\varepsilon\kappa_{R_bD}^2}$.

Similarly, we analyze the asymptotic behavior for SRS scheme as the number of relays grows into infinity.

Corollary 4: The scaling laws for SRS scheme under the non-ideal and ideal conditions are given by

[4] SRS strategy can select a relay to maximize the SINR between any transmission link of $S \to R_m$ or $R_m \to D$. In this paper, we choose a relay to maximize the SINR from S to R_m.

$$\begin{aligned} P_{out}^{SRS,ni} = 1 - \Bigg[& \frac{2\lambda_{R_bD}}{C_7} e^{-\frac{\lambda_{R_bD} C_8}{C_7}} \sqrt{\frac{\beta_4}{\gamma_4}} K_1\left(2\sqrt{\beta_4\gamma_4}\right) + e^{-\lambda_{BR_b}E_2}\left(e^{-\lambda_{R_bD}\Theta_4} - e^{-\lambda_{R_bD}T_7}\right) - \frac{\pi u_4 \lambda_{R_bD}}{2Y_4 C_7} \sum_{l_4=0}^{Y_4} \sqrt{1-\delta_{l_4}^2} \\ & \times e^{-\frac{\lambda_{R_bD} C_8}{C_7} - \frac{2\beta_4}{u_4\left(\delta_{l_4}+1\right)} - \frac{u_4\gamma_4\left(\delta_{l_4}+1\right)}{2}} \Bigg] \Bigg[\frac{2\omega\lambda_{SR_b}}{C_5} e^{-\frac{\lambda_{SR_b}(s+1)C_6}{C_5}} \sqrt{\frac{\beta_3}{\gamma_3}} \times K_1\left(2\sqrt{\beta_3\gamma_3}\right) - \frac{\omega}{s+1} e^{-\lambda_{BS}E_1 - \lambda_{SR_b}(s+1)T_5} \\ & - \frac{\pi u_3 \omega \lambda_{SR_b}}{2Y_3 C_5} \sum_{l_3=0}^{Y_3} \sqrt{1-\delta_{l_3}^2} e^{-\frac{\lambda_{SR_b}(s+1)C_6}{C_5} - \frac{2\beta_3}{u_3\left(\delta_{l_3}+1\right)} - \frac{\gamma_3 u_3\left(\delta_{l_3}+1\right)}{2}} \Bigg] + e^{-\lambda_{BS}E_1}\left[1 - \left(1 - e^{-\lambda_{SR_b}\Theta_3}\right)^M\right] \end{aligned} \tag{31}$$

$$\begin{aligned} P_{out}^{SRS,id} = 1 - \Bigg[& \frac{2\lambda_{R_bD}}{C_{72}} \sqrt{\frac{\beta_4}{\gamma_{42}}} K_1\left(2\sqrt{\beta_4\gamma_{42}}\right) + e^{-\lambda_{BR_b}E_2}\left(e^{-\lambda_{R_bD}\Theta_{42}} - e^{-\lambda_{R_bD}T_{72}}\right) - \frac{\pi u_4 \lambda_{R_bD}}{2Y_4 C_{72}} \sum_{l_4=0}^{Y_4} \sqrt{1-\delta_{l_4}^2} \\ & \times e^{-\frac{2\beta_4}{u_4\left(\delta_{l_4}+1\right)} - \frac{u_4\gamma_{42}\left(\delta_{l_4}+1\right)}{2}} \Bigg] \Bigg[\frac{2\omega\lambda_{SR_b}}{C_{52}} \sqrt{\frac{\beta_3}{\gamma_{32}}} K_1\left(2\sqrt{\beta_3\gamma_{32}}\right) - \frac{\omega}{s+1} e^{-\lambda_{BS}E_1 - \lambda_{SR_b}(s+1)T_{52}} - \frac{\pi u_3 \omega \lambda_{SR_b}}{2Y_3 C_{52}} \sum_{l_3=0}^{Y_3} \sqrt{1-\delta_{l_3}^2} \\ & \times e^{-\frac{2\beta_3}{u_3\left(\delta_{l_3}+1\right)} - \frac{\gamma_{32} u_3\left(\delta_{l_3}+1\right)}{2}} \Bigg] + e^{-\lambda_{BS}E_1}\left[1 - \left(1 - e^{-\lambda_{SR_b}\Theta_{32}}\right)^M\right] \end{aligned} \tag{32}$$

1) when $\Pr\left\{C_{SR_b}^j < C_{th}\right\} = 0$

- *Non-ideal conditions*

$$d_{ni}^{SRS} = 0, \tag{34}$$

- *Ideal conditions*

$$d_{id}^{SRS} = 0, \tag{35}$$

2) when $\Pr\left\{C_{R_bD}^j < C_{th}\right\} = 0$

- *Non-ideal conditions*

$$d_{ni}^{SRS} = -\log\left(\frac{1}{\Pr\left\{C_{SR_b}^{ni} < C_{th}\right\}}\right), \tag{36}$$

- *Ideal conditions*

$$d_{id}^{SRS} = -\log\left(\frac{1}{\Pr\left\{C_{SR_b}^{id} < C_{th}\right\}}\right), \tag{37}$$

Proof: In this case, substituting (B.3) into (26), we can obtain the following expression is

$$d_j^{SRS} = \lim_{M\to\infty} \frac{\log\left(\Pr\left\{\min\left(C_{SR_b}^j, C_{R_bD}^j\right) < C_{th}\right\}\right)}{M}. \tag{38}$$

The (B.3) can be rewritten as

$$\begin{aligned} P_{out}^{SRS,j} = & \left(\Pr\left\{C_{SR_b}^j < C_{th}\right\}\right)^M + \Pr\left\{C_{R_bD}^j < C_{th}\right\} \\ & - \left(\Pr\left\{C_{SR_b}^j < C_{th}\right\}\right)^M \left(\Pr\left\{C_{R_bD}^j < C_{th}\right\}\right), \end{aligned} \tag{39}$$

in this case, the dominant terms of (39) is

$$P_{out}^{SRS,j} = \left(\Pr\left\{C_{SR_b}^j < C_{th}\right\}\right)^M + \Pr\left\{C_{R_bD}^j < C_{th}\right\}, \tag{40}$$

substituting (40) into (38), we can get the expressions of (34), (35), (36) and (37). □

*Remark 2: The above **Corollary 4**, shows that:1) when* $\Pr\left\{C_{SR_b}^j < C_{th}\right\} = 0$*, for M is a large value, the scaling laws of OP approaches zero in both ideal and non-ideal cases. This means that for the SRS scheme, the system outage performance is independent of the number of relays in this case. 2) when* $\Pr\left\{C_{R_bD}^j < C_{th}\right\} = 0$ *and* $0 < \Pr\left\{C_{SR_b}^j < C_{th}\right\} < 1$*, for M is a large value, the scaling law for SRS scheme expressed as logarithmic scale. With the increases of M, the OP decreases and tends to a fixed value gradually; when* $\Pr\left\{C_{R_bD}^j < C_{th}\right\} = 0$ *and* $\Pr\left\{C_{SR_b}^j < C_{th}\right\} = 1$*, the slope is zero, meaning that outage performance is independent of the number of relays.*

3) ORS

For ORS scheme, the optimal relay is selected for the largest effective end-to-end channel capacity of communication, and it can be expressed as

$$m^* = \arg\max_{1\le m\le M} \min\left(C_{SR_m}, C_{R_mD}\right), \tag{41}$$

$$C_{R_{m^*}} = \max_{1\le m\le M} C_{R_m}. \tag{42}$$

Based on the above definitions, for OP of ORS scheme is discussed in the following theorem.

Theorem 3: The exact analytical expressions for OP of ORS scheme under non-ideal and ideal conditions are provided in (43) and (44), as shown at the top of the next page.

Proof: See Appendix C. □

Similar to **Corollary 1**, the following asymptotic expressions for ORS scheme can be obtained.

$$
\begin{aligned}
P_{out}^{ORS,ni} = & \prod_{m=1}^{M}\Bigg\{1-\Bigg[\frac{2\lambda_{SR_m}}{C_1}e^{-\frac{\lambda_{SR_m}C_2}{C_1}}\sqrt{\frac{\beta_1}{\gamma_1}}\,K_1\left(2\sqrt{\beta_1\gamma_1}\right)+e^{-\lambda_{BS}E_1}\left(e^{-\lambda_{SR_m}\Theta_1}-e^{-\lambda_{SR_m}T_1}\right)-\frac{\lambda_{SR_m}}{C_1}e^{-\frac{\lambda_{SR_m}C_2}{C_1}}\frac{\pi u_1}{2Y_1}\sum_{l_1=0}^{Y_1}\sqrt{1-\delta_{l_1}^2} \\
& \times\, e^{-\frac{2\beta_1}{u_1\left(\delta_{l_1}+1\right)}-\frac{u_1\gamma_1\left(\delta_{l_1}+1\right)}{2}}\Bigg]\Bigg[\frac{2\lambda_{R_mD}}{C_3}e^{-\frac{\lambda_{R_mD}C_4}{C_3}}\sqrt{\frac{\beta_2}{\gamma_2}}\,K_1\left(2\sqrt{\beta_2\gamma_2}\right)+e^{-\lambda_{BR_m}E_2}\left(e^{-\lambda_{R_mD}\Theta_2}-e^{-\lambda_{R_mD}T_3}\right) \\
& -\frac{\lambda_{R_mD}}{C_3}e^{-\frac{\lambda_{R_mD}C_4}{C_3}}\frac{\pi u_2}{2Y_2}\sum_{l_2=0}^{Y_2}\sqrt{1-\delta_{l_2}^2}\times e^{-\frac{2\beta_2}{u_2\left(\delta_{l_2}+1\right)}-\frac{u_2\gamma_2\left(\delta_{l_2}+1\right)}{2}}\Bigg]\Bigg\}
\end{aligned} \tag{43}
$$

$$
\begin{aligned}
P_{out}^{ORS,id} = & \prod_{m=1}^{M}\Bigg\{1-\Bigg[\frac{2\lambda_{SR_m}}{C_{12}}\sqrt{\frac{\beta_1}{\gamma_{12}}}\,K_1\left(2\sqrt{\beta_1\gamma_{12}}\right)+e^{-\lambda_{BS}E_1}\left(e^{-\lambda_{SR_m}\Theta_{12}}-e^{-\lambda_{SR_m}T_{12}}\right)-\frac{\lambda_{SR_m}}{C_{12}}\frac{\pi u_1}{2Y_1}\sum_{l_1=0}^{Y_1}\sqrt{1-\delta_{l_1}^2} \\
& \times\, e^{-\frac{2\beta_1}{u_1\left(\delta_{l_1}+1\right)}-\frac{u_1\gamma_{12}\left(\delta_{l_1}+1\right)}{2}}\Bigg]\Bigg[\frac{2\lambda_{R_mD}}{C_{32}}\sqrt{\frac{\beta_2}{\gamma_{22}}}\,K_1\left(2\sqrt{\beta_2\gamma_{22}}\right)+e^{-\lambda_{BR_m}E_2}\left(e^{-\lambda_{R_mD}\Theta_{22}}-e^{-\lambda_{R_mD}T_{32}}\right) \\
& -\frac{\lambda_{R_mD}}{C_{32}}\frac{\pi u_2}{2Y_2}\sum_{l_2=0}^{Y_2}\sqrt{1-\delta_{l_2}^2}\times e^{-\frac{2\beta_2}{u_2\left(\delta_{l_2}+1\right)}-\frac{u_2\gamma_{22}\left(\delta_{l_2}+1\right)}{2}}\Bigg]\Bigg\}
\end{aligned} \tag{44}
$$

Corollary 5: The asymptotic analysis for OP of ORS scheme under non-ideal conditions is given by

$$P_{out}^{ORS,\infty}=\prod_{i=1}^{M}\left(1-e^{-\lambda_{SR_m}\Theta_{A_1}-\lambda_{R_mD}\Theta_{A_2}}\right), \tag{45}$$

Similarly, the asymptotic behavior analysis of ORS scheme is analyzed as follows.

Corollary 6: The scaling laws for ORS scheme are given by

- *Non-ideal conditions*

$$d_{ni}^{ORS}=-\log\left(\frac{1}{\Pr\left\{\min\left(C_{SR_m}^{ni},C_{R_mD}^{ni}\right)<C_{th}\right\}}\right). \tag{46}$$

- *Ideal conditions*

$$d_{id}^{ORS}=-\log\left(\frac{1}{\Pr\left\{\min\left(C_{SR_m}^{id},C_{R_mD}^{id}\right)<C_{th}\right\}}\right). \tag{47}$$

Proof: Substituting (C.1) into (26), we can obtain the following expression is

$$
\begin{aligned}
d_j^{ORS} & =\lim_{M\to\infty}\frac{\log\left(\Pr\left\{\max\limits_{m=1,2,\cdots M}\left[\min\left(C_{SR_m}^{j},C_{R_mD}^{j}\right)\right]<C_{th}\right\}\right)}{M} \\
& =\lim_{M\to\infty}\frac{\log\left(\Pr\left\{\min\left(C_{SR_m}^{j},C_{R_mD}^{j}\right)<C_{th}\right\}\right)^M}{M} \\
& =-\lim_{M\to\infty}\frac{M\log\left(\Pr\left\{\min\left(C_{SR_m}^{j},C_{R_mD}^{j}\right)<C_{th}\right\}\right)^{-1}}{M} \\
& =-\log\left(\frac{1}{\Pr\left\{\min\left(C_{SR_m}^{j},C_{R_mD}^{j}\right)<C_{th}\right\}}\right).
\end{aligned} \tag{48}
$$

□

*Remark 3: The **Corollary 6** shows that: 1) when $0<\Pr\left\{\min\left(C_{SR_m}^{j},C_{R_mD}^{j}\right)<C_{th}\right\}<1$, the scaling law slope of OP for ORS scheme decreases as the number of relays M increases, for M is a large value, the result is expressed as logarithmic scale; meaning that the outage performance improves as the number of relays increases; 2) when $\Pr\left\{\min\left(C_{SR_m}^{j},C_{R_mD}^{j}\right)<C_{th}\right\}=1$, the slope is zero, meaning that outage performance is independent of the number of relays.*

B. INTERCEPT PROBABILITY ANALYSIS

In this subsection, we investigate the security performance of the multi-relay networks in terms of IP, where two scenarios are considered, i.e., non-colluding and colluding eavesdroppers.

Intercept Probability: IP is defined as the probability that the channel capacity of $R_m \to E_k$ is greater than the threshold C_{th}. Since the relay has been selected, the IP can be expressed as [21]

$$P_{int}\triangleq\Pr\left\{C_{R_cE_k}>C_{th}\right\}, \tag{49}$$

where R_c is the selected relay, and $C_{R_cE_k}$ is the intercept capacity of $R_c \to E_k$.

1) NON-COLLUDING EAVESDROPPERS

For non-colluding scenario, eavesdroppers are worked independently and each eavesdropper tries to decode the legitimate signal transmitted from relay individually. To this end, the eavesdropper that maximizes the eavesdropping capacity is selected. Therefore, the corresponding mathematical expression is

$$d = \arg \max_{1 \le k \le K} C_{R_c E_k}. \tag{50}$$

Based on the above definition, the IP expressions of (51) and (52) for non-colluding eavesdroppers scheme are presented in the following theorem.

Theorem 4: The exact analytical expressions for IP of non-colluding eavesdroppers scheme under non-ideal and ideal conditions are provided in (51) and (52), as shown at the bottom of this page, where $\omega_2 = K \sum_{g=0}^{K-1} \binom{K-1}{g} (-1)^g$, $W_1 = A_2 P_B \left(1 - \varepsilon \kappa_{R_c E_d}^2\right)$, $W_2 = \varepsilon A_2 P_B \sigma_{e_{R_c E_d}}^2 \left(1 + \kappa_{R_c E_d}^2\right)$, $O_1 = \frac{\varepsilon N_{R_c E_d}}{W_1 E_2} + \frac{W_2}{W_1}$, $u_5 = \frac{\varepsilon N_{R_c E_d}}{E_2}$, $\beta_5 = \lambda_{BR_c} \varepsilon N_{R_c E_d}$, $\gamma_5 = \frac{\lambda_{R_c E_d}(g+1)}{W_1}$, $\delta_{l_5} = \cos\left[\frac{(2l_5-1)\pi}{2Y_5}\right]$, $\Theta_5 = \frac{\varepsilon A_2 \Gamma_2 \sigma_{e_{R_b E_c}}^2 \left(1+\kappa_{R_b E_c}^2\right) + \varepsilon N_{R_b E_c}}{A_2 \Gamma_2 \left(1 - \varepsilon \kappa_{R_b E_c}^2\right)}$, $W_{12} = A_2 P_B$, $O_{12} = \frac{\varepsilon N_{R_c E_d}}{W_{12} E_2}$, $u_5 = \frac{\varepsilon N_{R_c E_d}}{E_2}$, $\beta_5 = \lambda_{BR_c} \varepsilon N_{R_c E_d}$, $\gamma_5 = \frac{\lambda_{R_c E_d}(g+1)}{W_1}$, $\delta_{l_5} = \cos\left[\frac{(2l_5-1)\pi}{2Y_5}\right]$, $\gamma_{52} = \frac{\lambda_{R_c E_d}(g+1)}{W_{12}}$ *and* $\Theta_{52} = \frac{\varepsilon N_{R_b E_c}}{A_2 \Gamma_2}$.

2) COLLUDING EAVESDROPPERS

The colluding eavesdroppers scheme is investigated and the eavesdroppers collaborate in order to intercept legitimate information. Using the MRC approach [52], the SINR of $R_c \to E_k$ is

$$\gamma_{R_c E_k}^{total} = \sum_{k=1}^{K} \gamma_{R_c E_k}. \tag{53}$$

We assume that the SINR of each intercept channel for collaborative eavesdropper is independent and identical, so we can get the following[5]

$$\gamma_{R_c E_k}^{total} = K \gamma_{R_c E_k}. \tag{54}$$

According to the definition of (49), the IP expressions of (55) and (56) for colluding eavesdroppers scheme are derived in the following theorem.

Theorem 5: The exact analytical expressions for IP of colluding eavesdroppers scheme under non-ideal and ideal conditions are provided in (55) and (56), as shown at the bottom of this page, where $\Xi = \frac{\varepsilon}{K}$, $W_3 = A_2 P_B \left(1 - \Xi \kappa_{R_c E_k}^2\right)$, $W_4 = \Xi A_2 P_B \sigma_{e_{R_c E_k}}^2 \left(1 + \kappa_{R_c E_k}^2\right)$, $O_2 = \frac{\Xi N_{R_c E_k}}{W_3 E_2} + \frac{W_4}{W_3}$, $u_6 = \frac{\Xi N_{R_c E_k}}{E_2}$, $\beta_6 = \lambda_{BR_c} \Xi N_{R_c E_k}$, $\gamma_6 = \frac{\lambda_{R_c E_k}}{W_3}$, $\delta_{l_6} = \cos\left[\frac{(2l_6-1)\pi}{2Y_6}\right]$, $\Theta_6 = \frac{\Xi A_2 \Gamma_2 \sigma_{e_{R_c E_k}}^2 \left(1+\kappa_{R_c E_k}^2\right) + \Xi N_{R_c E_k}}{A_2 \Gamma_2 \left(1 - \Xi \kappa_{R_c E_k}^2\right)}$, $W_{32} = A_2 P_B$, $O_{22} = \frac{\Xi N_{R_c E_k}}{W_{32} E_2}$, $\gamma_{62} = \frac{\lambda_{R_c E_k}}{W_{32}}$ *and* $\Theta_{62} = \frac{\Xi N_{R_c E_k}}{A_2 \Gamma_2}$.

Proof: See Appendix D. □

It is worth noting that substituting (50) and (53) into (49), respectively. Firstly, it can be seen that the security of colluding scenario outperform that of non-colluding scenario because of sharing information among eavesdroppers. As the number of eavesdroppers increases, more information can be intercepted, and the IP will increase for the two scenarios. In addition, the IP for non-ideal conditions is lower than that

[5]In fact, SINRs for all eavesdroppers are different since different eavesdroppers are, in general geographically separated. To maintain mathematical tractability and obtain engineering insights, we have adopted this simplified.

$$\begin{aligned} P_{int,ni}^{nc} = {} & \frac{2\omega_2 \lambda_{R_c E_d}}{W_1} e^{-\frac{\lambda_{R_c E_d}(g+1)W_2}{W_1}} \sqrt{\frac{\beta_5}{\gamma_5}} K_1\left(2\sqrt{\beta_5 \gamma_5}\right) - \frac{\omega_2 \lambda_{R_c E_d}}{W_1} e^{-\frac{\lambda_{R_c E_d}(g+1)W_2}{W_1}} \frac{\pi u_5}{2Y_5} \sum_{l_5=0}^{Y_5} e^{-\frac{2\beta_5}{u_5\left(\delta_{l_5}+1\right)} - \frac{\gamma_5 u_5\left(\delta_{l_5}+1\right)}{2}} \sqrt{1-\delta_{l_5}^2} \\ & + e^{-\lambda_{BR_c} E_2} \left(\left[1 - \left(1 - e^{-\lambda_{R_c E_d} \Theta_5}\right)^K\right] - \frac{\omega_2}{(g+1)} e^{-\lambda_{R_c E_d}(g+1) O_1}\right) \end{aligned} \tag{51}$$

$$\begin{aligned} P_{int,id}^{nc} = {} & \frac{2\omega_2 \lambda_{R_c E_d}}{W_{12}} \sqrt{\frac{\beta_5}{\gamma_5}} K_1\left(2\sqrt{\beta_5 \gamma_5}\right) - \frac{\omega_2 \lambda_{R_c E_d}}{W_{12}} \frac{\pi u_5}{2Y_5} \sum_{l_5=0}^{Y_5} e^{-\frac{2\beta_5}{u_5\left(\delta_{l_5}+1\right)} - \frac{\gamma_5 u_5\left(\delta_{l_5}+1\right)}{2}} \sqrt{1-\delta_{l_5}^2} + e^{-\lambda_{BR_c} E_2} \\ & \times \left(\left[1 - \left(1 - e^{-\lambda_{R_c E_d} \Theta_{52}}\right)^K\right] - \frac{\omega_2}{(g+1)} e^{-\lambda_{R_c E_d}(g+1) O_{12}}\right) \end{aligned} \tag{52}$$

$$\begin{aligned} P_{int,ni}^{co} = {} & e^{-\lambda_{BR_c} E_2} \left(e^{-\lambda_{R_c E_k} \Theta_6} - e^{-\lambda_{R_c E_k} O_2}\right) - \frac{\lambda_{R_c E_k}}{W_3} e^{-\frac{\lambda_{R_c E_k} W_4}{W_3}} \frac{\pi u_6}{2Y_6} \sum_{i_6=0}^{Y_6} e^{-\frac{2\beta_6}{u_6\left(\delta_{l_6}+1\right)} - \frac{u_6 \gamma_6\left(\delta_{l_6}+1\right)}{2}} \sqrt{1-\delta_{l_6}^2} \\ & + \frac{2\lambda_{R_c E_k}}{W_3} e^{-\frac{\lambda_{R_c E_k} W_4}{W_3}} \sqrt{\frac{\beta_6}{\gamma_6}} K_1\left(2\sqrt{\beta_6 \gamma_6}\right) \end{aligned} \tag{55}$$

$$P_{int,id}^{co} = e^{-\lambda_{BR_c} E_2} \left(e^{-\lambda_{R_c E_k} \Theta_{62}} - e^{-\lambda_{R_c E_k} O_{22}}\right) - \frac{\lambda_{R_c E_k}}{W_{32}} \frac{\pi u_6}{2Y_6} \sum_{l_6=0}^{Y_6} e^{-\frac{2\beta_6}{u_6\left(\delta_{l_6}+1\right)} - \frac{u_6 \gamma_{62}\left(\delta_{l_6}+1\right)}{2}} \sqrt{1-\delta_{l_6}^2} + \frac{2\lambda_{R_c E_k}}{W_{32}} \sqrt{\frac{\beta_6}{\gamma_{62}}} K_1\left(2\sqrt{\beta_6 \gamma_{62}}\right) \tag{56}$$

of ideal conditions due to RHIs and CEEs. This means that RHIs and CEEs can improve the security performance of the considered systems.

IV. NUMERICAL RESULTS

In this section, we provide some numerical results to verify the correctness of the theoretical analysis in Section III. Unless otherwise specified, the system parameters considered in our evaluation are set as follows $N_{SR_m} = N_{R_mD} = N_{R_mE_k} = 1$, $\sigma^2_{e_{SR_m}} = \sigma^2_{e_{R_mD}} = \sigma^2_{e_{R_mE_k}} = \sigma^2_e$, $d_{BS} = d_{BR_m} = 0.1$, $d_{SR_m} = d_{R_mD} = d_{R_mE_k} = 1.5$, $\beta_i = \beta = 3$, $\kappa_{SR_m} = \kappa_{R_mD} = \kappa_{R_mE_k} = \kappa$.

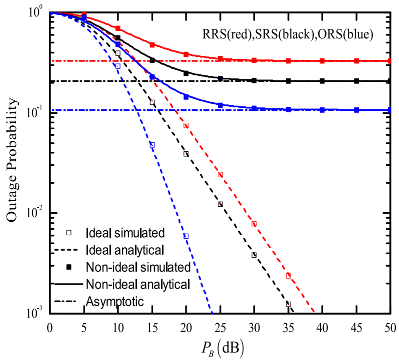

FIGURE 2. OP versus the transmit power for different RS schemes.

A. OUTAGE PROBABILITY

Fig. 2 plots the OP versus transmit power P_B under different RS schemes. In this simulation, we have set $\alpha = 0.5$, $C_{th} = 0.05$, $M = 2$, $\sigma^2_e = 0.05$, $\kappa = 0.1$, $\zeta_1 = 0.5$ and $\zeta_2 = 0.5$. For comparison, the outage performance of ideal conditions are provided with $\sigma^2_e = 0$ and $\kappa = 0$. It shows that OPs degrade as the transmit power of B increases. Comparing the OPs of RRS, SRS and ORS schemes, it can be observed that the outage performance of the RRS scheme is lower than that of SRS and ORS. This happens because that in contrast to RRS, SRS and ORS can provided extra diversity gain. Moreover, it can be also seen that there are error floors of OP for the proposed three schemes in the presence of RHIs and ICSI, which implies that RHIs and CEEs have a significant negative impact on system outage performance.

Fig. 3 shows the OPs under three RS schemes versus P_B for different estimation errors $\left(\sigma^2_e = 0, 0.05, 0.1\right)$. We have set $\alpha = 0.5$, $C_{th} = 0.05$, $M = 2$, $\kappa = 0.1$, $\zeta_1 = 0.5$ and $\zeta_2 = 0.5$. It can be seen that the value of OP becomes large as σ^2_e increases, which means that the larger estimation errors result in worse system reliability. We can also see that the OP performance is limited by CEE and there are error floors for the OP in the high SNR region. Moreover, the OP for the three RS schemes decreases linearly as the SNR grows large. This indicates that CEEs have a damaging effect on system outage performance.

As in [47], it is showed in Fig. 4 that the OPs versus transmit power at B for different levels of impairment ($\kappa = [0, 0.40]$). We have set the other parameters as $\alpha = 0.5$,

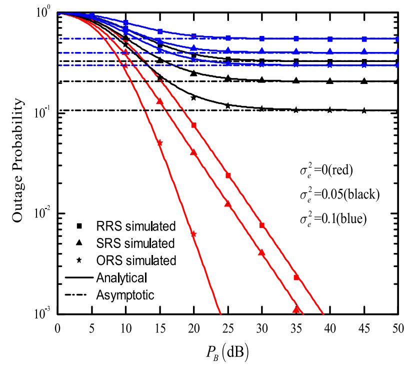

FIGURE 3. OP versus transmit power for different CEE parameters.

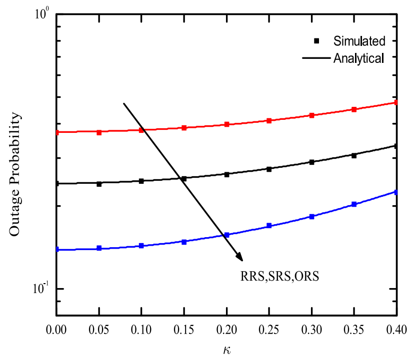

FIGURE 4. OP versus RHIs parameter for different RS schemes.

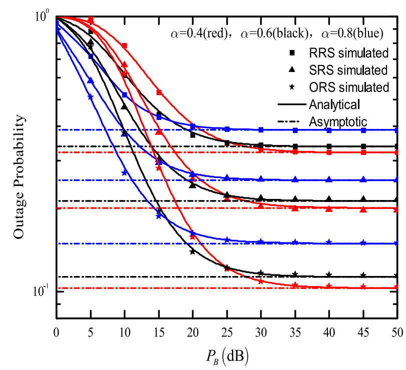

FIGURE 5. OP versus transmit power for different time allocation factors.

$C_{th} = 0.05$, $M = 2$, $\sigma^2_e = 0.05$, $\zeta_1 = 0.5$ and $\zeta_2 = 0.5$. It can be seen from the simulation that the reliability degrades as κ increases because of the impairments, that is, as the level of impairment increases, the OP increases. This means that the RHIs have a negative impact on the system.

Fig. 5 presents the OP versus P_B for the different time allocation factor ($\alpha = 0.4, 0.6, 0.8$). In this simulation, we have set $C_{th} = 0.05$, $M = 2$, $\sigma^2_e = 0.05$, $\kappa = 0.1$, $\zeta_1 = 0.5$ and $\zeta_2 = 0.5$. From Fig. 5, it can be seen that the outage performance gradually deteriorates from ORS, SRS and RRS. It can also be concluded that: 1) in the case of low transmit power, with the increases of α, the outage performance of the system gradually becomes better; 2) in the range of [15dB:20dB], the outage performance at $\alpha = 0.4$ is worse than that at

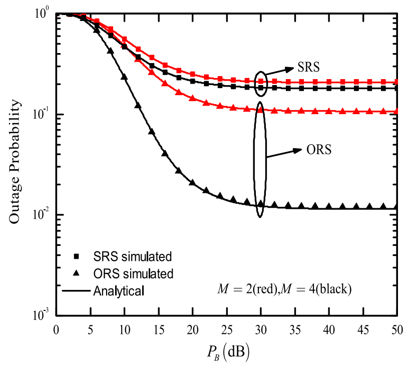

FIGURE 6. OP versus transmit power for different relay number.

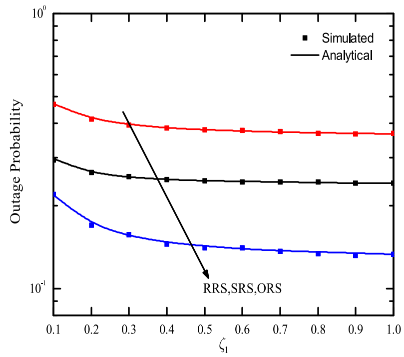

FIGURE 7. OP versus ζ_1 for different RS schemes.

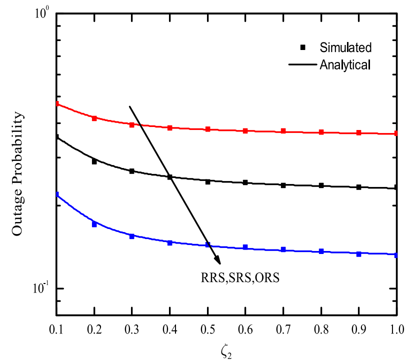

FIGURE 8. OP versus ζ_2 for different RS schemes.

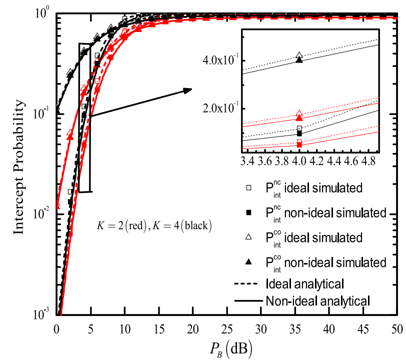

FIGURE 9. IP versus transmit power for different eavesdroppers number.

$\alpha = 0.6$ and 0.8, and the OP at $\alpha = 0.8$ is higher than that at $\alpha = 0.6$. This happens because that when $\alpha = 0.4$, there is not enough energy from B to support transmission; 3) in the range of [20dB:25dB], the system performance at $\alpha = 0.8$ is worse than that at $\alpha = 0.4$ and $\alpha = 0.6$, while the system performance at $\alpha = 0.4$ is worse than that at $\alpha = 0.6$; 4) in the high transmit power, the OP of the system increases with the increases of α.

Fig. 6 depicts the OPs under SRS and ORS schemes versus transmit power for different relay number ($M = 2, 4$). In this simulation, we have set the parameters as $\alpha = 0.5, C_{th} = 0.05, M = 2, \sigma_e^2 = 0.05$ and $\kappa = 0.1$. It shows that the OP decreases as the number of relay increases, that is, as the M increases, the overall performance of the system becomes better. Moreover, deploying multi-relay for ORS scheme can achieve more OP gain than that of SRS scheme.

In Figs. 7 and 8, we plot the OP versus the energy conversion efficiency for the proposed RS schemes. In the simulation, we have set $\alpha = 0.5, C_{th} = 0.05, M = 2, \sigma_e^2 = 0.05, \kappa = 0.1$ and $\zeta_1 = \zeta_2 = 0.5$. From Figs. 7 and 8, we can observe that high energy conversion efficiency factor obtain better system outage performance. This happens because more energy can be harvested by source and relay for the transmission phase.

B. INTERCEPT PROBABILITY

Fig. 9 presents that the IP versus transmit power P_B with different eavesdroppers number ($K = 2, 4$). In this simulation, we have set $C_{th} = 0.05, M = 2, \sigma_e^2 = 0.05, \kappa = 0.1$ and $\zeta_1 = \zeta_2 = 0.5$. It reveals that the system security performance is gradually improved as the number of eavesdroppers increases. In addition, it is shown that the IP under various eavesdropping connection modes (non-colluding eavesdroppers, colluding eavesdroppers) is proportional to P_B. Comparing IP in two cases:1) ideal conditions: $\sigma_e^2 = 0$ and $\kappa = 0$; 2) non-ideal conditions: $\sigma_e^2 = 0.05$ and $\kappa = 0.1$, the IP in the former case is larger than that of latter one. This means that the ideal communication network is more vulnerable to eavesdropping than that of non-ideal communication network. At the same time, the eavesdropping connection cases under different circumstances are compared, and the IP in the case of non-colluding eavesdroppers is lower than that in case of colluding eavesdroppers. These simulation results firmly verify the expressions of (51), (52), (55) and (56).

In Fig. 10, the IP versus eavesdroppers number K for different target rates ($C_{th} = 0.1, 0.5$) is studied. We have set $P_B = 5dB, \alpha = 0.5, \sigma_e^2 = 0.05, \kappa = 0.1, \zeta_1 = 0.5$ and $\zeta_2 = 0.5$. For the two conditions of non-colluding and colluding eavesdroppers, it can be seen that IP becomes larger with the number of eavesdropper, K. Meanwhile, IP is inversely proportional to the target rate. It can be understood from the simulation that the IP reduces with the rises of C_{th}. When the target rate is higher, the IP difference between colluding and non-colluding eavesdroppers is larger.

Fig. 11 plots IP versus transmit power P_B for different estimation errors $\left(\sigma_e^2 = 0, 0.05, 0.1\right)$. In this simulation,

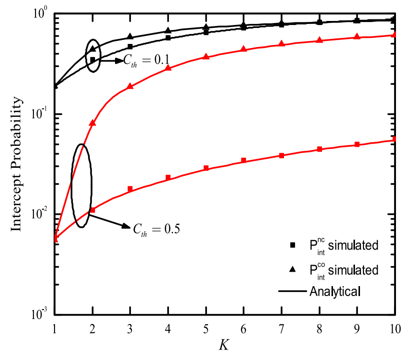

FIGURE 10. IP versus eavesdroppers number for different C_{th}.

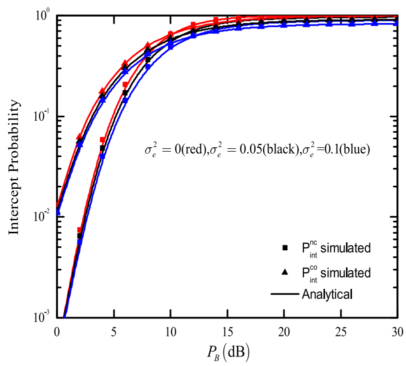

FIGURE 11. IP versus transmit power for different CEE parameters.

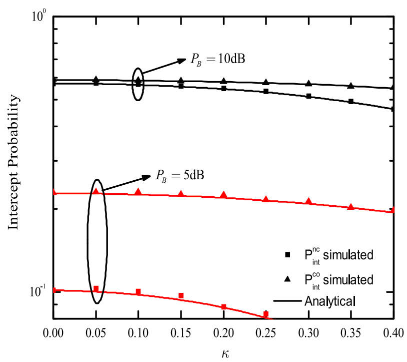

FIGURE 12. IP versus RHIs parameter for different transmit power.

the parameters are set as $\alpha = 0.3, C_{th} = 0.05, K = 2$, $\kappa = 0.1$, $\zeta_1 = 0.5$ and $\zeta_2 = 0.5$. We can observe that when σ_e^2 is increased, the IPs of the system under the two eavesdropping connection modes are weakened due to the CEEs. Meanwhile, the simulation also proves that for the different σ_e^2, the IPs of the communication networks under colluding eavesdroppers is larger than that the non-colluding case since the information can be shared under the condition of colluding case. Finally, It is also can be seen that at low SNR, the effects of CEEs on the IP of the two cases can be ignored.

Fig. 12 plots the IP versus the levels of impairment for different transmit power: 1) $P_B = 5dB$; 2) $P_B = 10dB$. We have set the other parameters as $\alpha = 0.3, C_{th} = 0.05, K = 2$, $\sigma_e^2 = 0.05$ and $\zeta_2 = 0.5$. We take the range of the transceiver impairment level of $\kappa \in [0, 0.40]$.[6] From Fig. 12, we can observe that the IP decreases as κ increases. This means that the system's eavesdropping performance is inversely proportional to the levels of impairments and the difference for the IP between colluding and non-colluding eavesdroppers becomes large as κ increases. Comparing the two different transmit power, it is found that for larger transmit SNR, the eavesdroppers can achieve higher IP performance, and the difference for the IP between the two eavesdropping connection modes is small for the large transmit SNR.

Fig. 13 shows that the IPs of non-colluding and colluding eavesdroppers increase as ζ_2 grows large. This is because relay nodes can harvest more energy for secure communication under the case of larger energy conversion coefficient. In this simulation, we have set $P_B = 5dB, \alpha = 0.3, C_{th} = 0.05, K = 2, \sigma_e^2 = 0.05$ and $\kappa = 0.1$. It is also implied that the value of α is proportional to the IP of the system at $P_B = 5dB$.

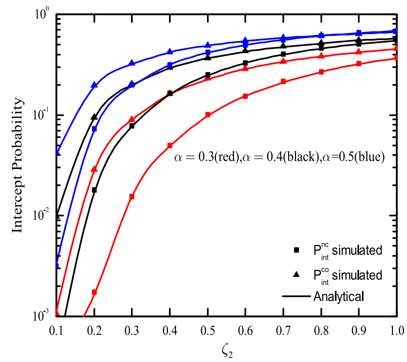

FIGURE 13. IP versus ζ_2 for different time allocation factors.

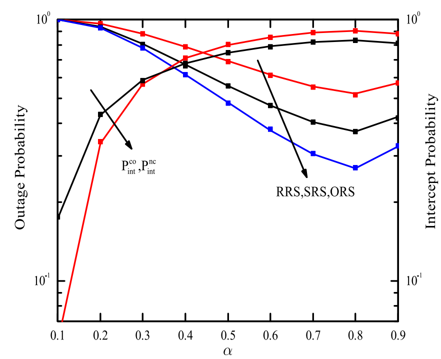

FIGURE 14. IP versus time allocation factor for different connection strategies.

Fig. 14 plots the IP versus α for different connection strategies. In this simulation, we have set $P_B = 10dB$,

[6]For HIs, 3GPP LTE has EVM requirements in the range $\kappa \in [0.08, 0.175]$. However, here we set $\kappa \in [0, 0.40]$ in order to better understand the impact of changes in RHIs parameters on system security.

$C_{th} = 0.05, K = 2, \sigma_e^2 = 0.05, \kappa = 0.1$ and $\zeta_2 = 0.5$. From Fig. 14, we can observe that the OP for the proposed RS schemes first increases and then decreases when the value of α grows large, while the IPs for the two eavesdropping connection modes always increase across the entire range of α. This means that there is an optimal α to maximize the OP. IPs of non-colluding eavesdroppers and colluding eavesdroppers become large. In addition, it can be further obtained that optimal α to obtain a balanced trade-off between the reliability and security of the considered system.

V. CONCLUSION

In this paper, we proposed a DF relays network considering HIs, imperfect CSI and nonlinear energy harvester. Based on the model, we firstly derived the closed-form analytical expressions of the OP for RRS, SRS and ORS schemes and IP for non-colluding and colluding eavesdroppers strategies. In order to obtain more insights, we further discussed the asymptotic OP at high SNRs and the scaling laws as the number of relays approaches to infinity. Numerical results illustrated that: 1) under the RRS and SRS schemes, the secure performance of system in the presence of ideal condition is better than the non-ideal condition; comparing the three RS schemes, the system performance under the ORS scheme outperform the other RS strategies, and the performance under the RRS scheme is the worst; 2) although CEEs and distortion noise have negative effects on the reliability of the considered system for the three RS schemes, it can enhance system security for the two eavesdropping connection modes; 3) the outage performance of the system is proportional to the number of relay; when the M value is sufficiently large, the OP under SRS strategy gradually becomes saturated; 4) when the energy conversion efficiencies become larger, the reliability performance of the system is improved; 5) the system's eavesdropping ability is proportional to the number of eavesdropper; 6) the IP of the system degrades as C_{th} becomes larger.

In future work, multi-antenna technique can be introduced into our considered system to further improve the reliability and security performance. In addition, our analysis can be extend to more general fading channels, such as Nakagami-m fading channel and Rician fading channel, which are set as our future work [56].

APPENDIX A: PROOF OF THEOREM 1

Substituting (18) into (19), we can obtained the following:

$$\begin{aligned} P_{out}^{RRS} &= \Pr\left\{\min\left(C_{SR_m}, C_{R_mD}\right) < C_{th}\right\} \\ &= 1 - \underbrace{\Pr\left\{C_{SR_m} > C_{th}\right\}}_{I_1}\underbrace{\Pr\left\{C_{R_mD} > C_{th}\right\}}_{I_2}. \end{aligned} \tag{A.1}$$

Set $\varepsilon = 2^{\frac{2C_{th}}{1-\alpha}} - 1$, we calculate I_1 and I_2 in the following calculations.

Firstly, put (15) into (A.1), the mathematical calculation of I_1 as follows:

$$\begin{aligned} I_1 &= \Pr\left\{C_{SR_m} > C_{th}\right\} \\ &= \Pr\left\{\frac{1-\alpha}{2}\log_2 \right. \\ &\quad \left. \times\left(1+\frac{\rho_{SR_m}\left|\hat{h}_{SR_m}\right|^2}{\rho_{SR_m}\left|\hat{h}_{SR_m}\right|^2\kappa_{SR_m}^2+\rho_{SR_m}\sigma_{eSR_m}^2\left(1+\kappa_{SR_m}^2\right)+1}\right)>C_{th}\right\} \\ &= \Pr\left\{\frac{\rho_{SR_m}\left|\hat{h}_{SR_m}\right|^2}{\rho_{SR_m}\left|\hat{h}_{SR_m}\right|^2\kappa_{SR_m}^2+\rho_{SR_m}\sigma_{eSR_m}^2\left(1+\kappa_{SR_m}^2\right)+1} > \varepsilon\right\} \\ &= \Pr\left\{\left|\hat{h}_{SR_m}\right|^2 > \frac{\varepsilon P_S\sigma_{eSR_m}^2 + \varepsilon P_S\sigma_{eSR_m}^2\kappa_{SR_m}^2 + \varepsilon N_{SR_m}}{P_S\left(1-\varepsilon\kappa_{SR_m}^2\right)}\right\} \\ &= M_1 + M_2, \end{aligned} \tag{A.2}$$

where

$$M_1 = \Pr\left\{|h_{BS}|^2\left(C_1\left|\hat{h}_{SR_m}\right|^2 - C_2\right) \geq \varepsilon N_{SR_m}, |h_{BS}|^2 \leq E_1\right\}, \tag{A.3}$$

and

$$M_2 = \Pr\left\{\left|\hat{h}_{SR_m}\right|^2 > \Theta_1, |h_{BS}|^2 > E_1\right\}, \tag{A.4}$$

in which, $T_2 = \frac{\varepsilon N_{SR_m}}{C_1\left|\hat{h}_{SR_m}\right|^2 - C_2}$.

By further calculation, we can get the M_1 and M_2 as following:

$$\begin{aligned} M_1 &= \Pr\left\{T_2 \leq |h_{BS}|^2 \leq E_1, \left|\hat{h}_{SR_m}\right|^2 \geq T_1\right\} \\ &= \int_{T_1}^{\infty}\int_{T_2}^{E_1} f_{|h_{BS}|^2}(x) f_{\left|\hat{h}_{SR_m}\right|^2}(y)dxdy, \end{aligned} \tag{A.5}$$

plugging in the PDF expressions of Rayleigh distribution into (A.5), we can obtain the following expressions as:

$$\begin{aligned} M_1 &= \int_{T_1}^{\infty}\int_{T_2}^{E_1} \lambda_{BS}e^{-\lambda_{BS}x}\lambda_{SR_m}e^{-\lambda_{SR_m}y}dxdy \\ &= -\lambda_{SR_m}\left[e^{-\lambda_{BS}E_1}\underbrace{\int_{T_1}^{\infty}e^{-\lambda_{SR_m}y}dy}_{\theta_1} - \underbrace{\int_{T_1}^{\infty}e^{-\frac{\lambda_{BS}\varepsilon N_{SR_m}}{C_1 y - C_2} - \lambda_{SR_m}y}dy}_{\theta_2}\right] \\ &= -\lambda_{SR_m}\left[e^{-\lambda_{BS}E_1}\theta_1 - \theta_2\right] \\ &= -e^{-\lambda_{BS}E_1 - \lambda_{SR_m}T_1} + \lambda_{SR_m}\theta_2, \end{aligned} \tag{A.6}$$

θ_2 can be obtained by the (3.324.1) in [53] and the Gaussian-Chebyshev quadrature [54]. Specifically, the integral in (A.6) is approximated as follows:

$$\int_0^u g(x)dx \approx \frac{\pi\beta}{2Y}\sum_{l=0}^{Y} g\left(\frac{\beta(\delta_l+1)}{2}\right)\sqrt{1-\delta_l^2}, \quad (A.7)$$

according to the equation (A.7), set $u = C_1T_1 - C_2$, we can obtain the θ_2 is:

$$\begin{aligned}\theta_2 &\overset{z=C_1y-C_2}{=} \frac{1}{C_1}\int_{C_1T_1-C_2}^{\infty} e^{-\frac{\lambda_{BS}\varepsilon N_{SR_m}}{z}-\frac{\lambda_{SR_m}(z+C_2)}{C_1}}dz\\ &= \frac{1}{C_1}\left(\int_0^{\infty} e^{-\frac{\lambda_{BS}\varepsilon N_{SR_m}}{z}-\frac{\lambda_{SR_m}(z+C_2)}{C_1}}dz\right.\\ &\quad\left.-\int_0^{u} e^{-\frac{\lambda_{BS}\varepsilon N_{SR_m}}{z}-\frac{\lambda_{SR_m}(z+C_2)}{C_1}}dz\right)\\ &= \frac{1}{C_1}\left[2e^{-\frac{\lambda_{SR_m}C_2}{C_1}}\sqrt{\frac{\beta_1}{\gamma_1}}K_1\left(2\sqrt{\beta_1\gamma_1}\right)\right.\\ &\quad\left.-e^{-\frac{\lambda_{SR_m}C_2}{C_1}}\frac{\pi u_1}{2Y_1}\sum_{l_1=0}^{Y_1} e^{-\frac{2\beta_1}{u_1(\delta_{l_1}+1)}-\frac{u_1\gamma_1(\delta_{l_1}+1)}{2}}\sqrt{1-\delta_{l_1}^2}\right],\end{aligned} \quad (A.8)$$

$$\begin{aligned}M_2 &= \Pr\left\{\left|\hat{h}_{SR_m}\right|^2 > \Theta_1\right\}\Pr\left\{|h_{BS}|^2 > E_1\right\}\\ &= \left(1-\Pr\left\{\left|\hat{h}_{SR_m}\right|^2 < \Theta_1\right\}\right)\left(1-\Pr\left\{|h_{BS}|^2 < E_1\right\}\right)\\ &= \left(1-F_{\left|\hat{h}_{SR_m}\right|^2}(\Theta_1)\right)\left(1-F_{|h_{BS}|^2}(E_1)\right).\end{aligned} \quad (A.9)$$

Substituting the CDF expressions of Rayleigh distribution into (A.9), the M_2 can be expressed as:

$$M_2 = e^{-\lambda_{SR_m}\Theta_1-\lambda_{BS}E_1}. \quad (A.10)$$

Substituting (A.6) and (A.9) into (A.2), and we can get I_1.

Secondly, put (16) into (A.1), the mathematical calculation of I_2 as follows:

$$\begin{aligned}I_2 &= \Pr\left\{C_{R_mD} > C_{th}\right\}\\ &= \Pr\left\{\frac{\rho_{R_mD}\left|\hat{h}_{R_mD}\right|^2}{\rho_{R_mD}\left|\hat{h}_{R_mD}\right|^2\kappa_{R_mD}^2+\rho_{R_mD}\sigma_{e_{R_mD}}^2\left(1+\kappa_{R_mD}^2\right)+1} > \varepsilon\right\}\\ &= \Pr\left\{\left|\hat{h}_{R_mD}\right|^2 > \frac{\varepsilon P_{R_m}\sigma_{e_{R_mD}}^2+\varepsilon P_{R_m}\sigma_{e_{R_mD}}^2\kappa_{R_mD}^2+\varepsilon N_{R_mD}}{P_{R_m}\left(1-\varepsilon\kappa_{R_mD}^2\right)}\right\}\\ &= M_3 + M_4.\end{aligned} \quad (A.11)$$

Similar to the calculation procedure and method of I_1, we can obtain M_3 and M_4 as following:

$$\begin{aligned}M_3 &= \frac{2\lambda_{R_mD}}{C_3}e^{-\frac{\lambda_{R_mD}C_4}{C_3}}\sqrt{\frac{\beta_2}{\gamma_2}}K_1\left(2\sqrt{\beta_2\gamma_2}\right)-e^{-\lambda_{BR_m}E_2-\lambda_{R_mD}T_3}\\ &\quad-\frac{\lambda_{R_mD}}{C_3}e^{-\frac{\lambda_{R_mD}C_4}{C_3}}\frac{\pi u_2}{2Y_2}\sum_{l_2=0}^{Y_2} e^{-\frac{2\beta_2}{u_2(\delta_{l_2}+1)}-\frac{u_2\gamma_2(\delta_{l_2}+1)}{2}}\sqrt{1-\delta_{l_2}^2},\end{aligned} \quad (A.12)$$

$$M_4 = e^{-\lambda_{R_mD}\Theta_2-\lambda_{BR_m}E_2}. \quad (A.13)$$

Substituting (A.12) and (A.13) into (A.11), we can get I_2. Then, put I_1 and I_2 into (A.1), (21) can be obtained.

Set $\kappa_{SR_m} = \kappa_{R_mD} = 0$ and $\sigma_{e_{SR_m}}^2 = \sigma_{e_{R_mD}}^2 = 0$, we can obtained the OP of ideal conditions, that is, we can get (22).

APPENDIX B: PROOF OF THEOREM 2

For SRS scheme, the CDF and PDF for $\left|\hat{h}_{SR_b}\right|^2$ are expressed as

$$F_{\left|\hat{h}_{SR_b}\right|^2}(y) = \left[1-e^{-\lambda_{SR_b}y}\right]^M, \quad (B.1)$$

$$f_{\left|\hat{h}_{SR_b}\right|^2}(y) = M\lambda_{SR_b}\sum_{s=0}^{M-1}\binom{M-1}{s}(-1)^s e^{-\lambda_{SR_b}(s+1)y}. \quad (B.2)$$

Substituting (30) into (19), we can obtain the following expression is

$$\begin{aligned}P_{out}^{SRS} &= \Pr\left\{\min\left(C_{SR_b}, C_{R_bD}\right) < C_{th}\right\}\\ &= 1-\underbrace{\Pr\left\{C_{SR_b} > C_{th}\right\}}_{I_3}\underbrace{\Pr\left\{C_{R_bD} > C_{th}\right\}}_{I_4}.\end{aligned} \quad (B.3)$$

Similar to the Appendix A, we calculate I_3 and I_4 in the following calculations.

In the first place, substituting (12) into (B.3), the correlation calculation of I_3 as follows:

$$\begin{aligned}I_3 &= \Pr\left\{\gamma_{SR_b} > \varepsilon\right\}\\ &= \Pr\left\{\frac{\left|\hat{h}_{SR_b}\right|^2 P_S}{P_S\sigma_{e_{SR_b}}^2+\left|\hat{h}_{SR_b}\right|^2 P_S\kappa_{SR_b}^2+P_S\sigma_{e_{SR_b}}^2\kappa_{SR_b}^2+N_{SR_b}} > \varepsilon\right\}\\ &= \Pr\left\{\left|\hat{h}_{SR_b}\right|^2 > \frac{\varepsilon P_S\sigma_{e_{SR_b}}^2+\varepsilon P_S\sigma_{e_{SR_b}}^2\kappa_{SR_b}^2+\varepsilon N_{SR_b}}{P_S\left(1-\varepsilon\kappa_{SR_b}^2\right)}\right\}\\ &= M_5 + M_6,\end{aligned} \quad (B.4)$$

where

$$M_5 = \Pr\left\{|h_{BS}|^2\left(C_5\left|\hat{h}_{SR_b}\right|^2-C_6\right) \geq \varepsilon N_{SR_b}, |h_{BS}|^2 \leq E_1\right\}, \quad (B.5)$$

and

$$M_6 = \Pr\left\{\left|\hat{h}_{SR_b}\right|^2 > \Theta_3, |h_{BS}|^2 > E_1\right\}, \quad (B.6)$$

in which, $T_6 = \frac{\varepsilon N_{SR_b}}{C_5\left|\hat{h}_{SR_b}\right|^2-C_6}$.

By further calculation, we can get the M_5 and M_6 as following:

$$M_6 = \Pr\left\{T_6 \leq |h_{BS}|^2 \leq E_1, \left|\hat{h}_{SR_b}\right|^2 \geq T_5\right\} = \int_{T_5}^{\infty}\int_{T_6}^{E_1} f_{|h_{BS}|^2}(x) f_{\left|\hat{h}_{SR_b}\right|^2}(y)dxdy, \quad (B.7)$$

substituting the PDF expression of Rayleigh distribution and (B.2) into (B.5), we can obtain the following expressions as:

$$M_5 = \int_{T_5}^{\infty}\int_{T_6}^{E_1} \omega\lambda_{BS} e^{-\lambda_{BS}x}\lambda_{SR_b} e^{-\lambda_{SR_b}(s+1)y}dxdy = \omega\lambda_{SR_b}\left[\underbrace{\int_{T_5}^{\infty} e^{-\lambda_{BS}T_6-\lambda_{SR_b}(s+1)y}dy}_{\theta_5} - e^{-\lambda_{BS}E_1}\underbrace{\int_{T_5}^{\infty} e^{-\lambda_{SR_b}(s+1)y}dy}_{\theta_6}\right]. \quad (B.8)$$

Similar to solving I_1, we can get M_5 and M_6 are

$$M_5 = \omega\lambda_{SR_b}\left[\theta_5 - e^{-\lambda_{BS}E_1}\theta_6\right], \quad (B.9)$$

$$M_6 = \left[1 - \left(1 - e^{-\lambda_{SR_b}\Theta_3}\right)^M\right] e^{-\lambda_{BS}E_1}, \quad (B.10)$$

where

$$\theta_5 = \frac{2}{C_5} e^{-\frac{\lambda_{SR_b}(s+1)C_6}{C_5}}\sqrt{\frac{\beta_3}{\gamma_3}} K_1\left(2\sqrt{\beta_3\gamma_3}\right) - \frac{1}{C_5} \times e^{-\frac{\lambda_{SR_b}(s+1)C_6}{C_5}}\frac{\pi u_3}{2Y_3}\sum_{l_3=0}^{Y_3} e^{-\frac{2\beta_3}{u_3\left(\delta_{l_3}+1\right)}-\frac{\gamma_3 u_3\left(\delta_{l_3}+1\right)}{2}}\sqrt{1-\delta_{l_3}^2}, \quad (B.11)$$

and

$$\theta_6 = \frac{1}{\lambda_{SR_b}(s+1)} e^{-\lambda_{SR_b}(s+1)T_5}. \quad (B.12)$$

Substituting (B.9) and (B.10) into (B.4), we can obtain I_3.

Then, substitute (16) into (B.3), the correlation calculation of I_4 as follows:

$$I_4 = \Pr\left\{\gamma_{R_bD} > \varepsilon\right\} = \Pr\left\{\frac{\left|\hat{h}_{R_bD}\right|^2 P_{R_b}}{P_{R_b}\sigma_{e_{R_bD}}^2 + \left|\hat{h}_{R_bD}\right|^2 P_{R_b}\kappa_{R_bD}^2 + P_{R_b}\sigma_{e_{R_bD}}^2\kappa_{R_bD}^2 + N_{R_bD}} > \varepsilon\right\} = \Pr\left\{\left|\hat{h}_{R_bD}\right|^2 > \frac{\varepsilon P_{R_b}\sigma_{e_{R_bD}}^2 + \varepsilon P_{R_b}\sigma_{e_{R_bD}}^2\kappa_{R_bD}^2 + \varepsilon N_{R_bD}}{P_{R_b}\left(1-\varepsilon\kappa_{R_bD}^2\right)}\right\} = M_7 + M_8. \quad (B.13)$$

Similar to the calculation procedure and method of I_1, we can obtain M_7 and M_8 as following:

$$M_7 = \frac{2\lambda_{R_bD}}{C_7} e^{-\frac{\lambda_{R_bD}C_8}{C_7}}\sqrt{\frac{\beta_4}{\gamma_4}} K_1\left(2\sqrt{\beta_4\gamma_4}\right) - e^{-\lambda_{BR_b}E_2-\lambda_{R_bD}T_5} - \frac{\lambda_{R_bD}}{C_7} e^{-\frac{\lambda_{R_bD}C_8}{C_7}}\frac{\pi u_4}{2Y_4}\sum_{l_4=0}^{Y_4} e^{-\frac{2\beta_4}{u_4(\delta_{l_4}+1)}-\frac{u_4\gamma_4(\delta_{l_4}+1)}{2}}\sqrt{1-\delta_{l_4}^2}, \quad (B.14)$$

$$M_8 = e^{-\lambda_{R_bD}\Theta_4-\lambda_{BR_b}E_2}. \quad (B.15)$$

Put (B.14) and (B.15) into (B.13), the I_4 can be obtained.

Substituting I_3 and I_4 into (B.3), the (31) can be obtained.

Set $\kappa_{SR_b} = \kappa_{R_bD} = 0$ and $\sigma_{e_{SR_b}}^2 = \sigma_{e_{R_bD}}^2 = 0$, we can obtained (32).

APPENDIX C: PROOF OF THEOREM 3

According to the definition of (42), for ORS strategy, the following expression can be obtained

$$P_{out}^{ORS} = \Pr\left\{C_{R_{m^*}} < R_{th}\right\} = \Pr\left\{\max_{m=1,2,\cdots M}\left[\min\left(\gamma_{SR_m}, \gamma_{R_mD}\right)\right] < \varepsilon\right\} = \prod_{m=1}^{M}(1 - I_1 I_2), \quad (C.1)$$

substituting I_1 and I_2 in Appendix A into (C.1), the (43) can be obtained.

Set $\kappa_{SR_m} = \kappa_{R_mD} = 0$ and $\sigma_{e_{SR_m}}^2 = \sigma_{e_{R_mD}}^2 = 0$, we can obtained the OP of ideal conditions, that is, we can get (44).

APPENDIX D: PROOFS OF THEOREM 4 AND THEOREM 5

A. NON-COLLUDING EAVESDROPPERS SCHEME

Putting (50) into (49), we can obtain the following formula is

$$P_{int,ni}^{nc} = \Pr\left\{C_{R_cE_d} > C_{th}\right\} = \Pr\left\{\frac{\left|\hat{h}_{R_cE_d}\right|^2 P_{R_c}}{P_{R_c}\sigma_{e_{R_cE_d}}^2 + \left|\hat{h}_{R_cE_d}\right|^2 P_{R_c}\kappa_{R_cE_d}^2 + P_{R_c}\sigma_{e_{R_cE_d}}^2\kappa_{R_cE_d}^2 + N_{R_cE_d}} > \varepsilon\right\} = \Pr\left\{\left|\hat{h}_{R_cE_d}\right|^2 > \frac{\varepsilon P_{R_c}\sigma_{e_{R_cE_d}}^2 + \varepsilon P_{R_c}\sigma_{e_{R_cE_d}}^2\kappa_{R_cE_d}^2 + \varepsilon N_{R_cE_d}}{P_{R_c}\left(1-\varepsilon\kappa_{R_cE_d}^2\right)}\right\} = Q_1 + Q_2, \quad (D.1)$$

and just like the calculation of I_3, we can derive the Q_1 and Q_2 in the following expressions are

$$Q_1 = \frac{2\omega_2\lambda_{R_cE_d}}{W_1} e^{-\frac{\lambda_{R_cE_d}(g+1)W_2}{W_1}}\sqrt{\frac{\beta_5}{\gamma_5}} K_1\left(2\sqrt{\beta_5\gamma_5}\right) - \frac{\omega_2\lambda_{R_cE_d}}{W_1} e^{-\frac{\lambda_{R_cE_d}(g+1)W_2}{W_1}}\frac{\pi u_5}{2Y_5}\sum_{l_5=0}^{Y_5} e^{-\frac{2\beta_5}{u_5(\delta_{l_5}+1)}-\frac{\gamma_5 u_5(\delta_{l_5}+1)}{2}} \times\sqrt{1-\delta_{l_5}^2} - \frac{\omega_2}{(g+1)} e^{-\lambda_{BR_c}E_2-\lambda_{R_cE_d}(g+1)O_1}, \quad (D.2)$$

$$Q_2 = \left[1-\left(1-e^{-\lambda_{R_cE_d}\Theta_5}\right)^K\right]e^{-\lambda_{BR_c}E_2}. \tag{D.3}$$

Put (D.2) and (D.3) into (D.1), we can obtain (51); set $\kappa_{R_cE_d}=0$ and $\sigma^2_{e_{R_cE_d}}=0$ we can derive the (52).

B. COLLUDING EAVESDROPPERS SCHEME

Substituting (54) into (50), we can further compute the following formula is

$$\begin{aligned}
&P^{co}_{int,ni}\\
&= \Pr\left\{\frac{1}{2}\log_2\left(1+K\gamma_{R_cE_k}\right) > C_{th}\right\}\\
&= \Pr\left\{\frac{\left|\hat{h}_{R_cE_k}\right|^2 P_{R_c}}{P_{R_c}\sigma^2_{e_{R_cE_k}}+\left|\hat{h}_{R_cE_k}\right|^2 P_{R_a}\kappa^2_{R_cE_k}+P_{R_c}\sigma^2_{e_{R_cE_k}}\kappa^2_{R_cE_k}+N_{R_cE_k}} > \Xi\right\}\\
&= \Pr\left\{\left|\hat{h}_{R_cE_k}\right|^2 > \frac{\Xi P_{R_c}\sigma^2_{e_{R_cE_k}}+\Xi P_{R_c}\sigma^2_{e_{R_cE_k}}\kappa^2_{R_cE_k}+\Xi N_{R_cE_k}}{P_{R_c}\left(1-\Xi\kappa^2_{R_cE_k}\right)}\right\}\\
&= Q_3+Q_4,
\end{aligned} \tag{D.4}$$

where $\Xi = \varepsilon/K$.

Similarly, the calculation method and steps of I_1. After calculation, we can get Q_3 and Q_4 are

$$\begin{aligned}
Q_3 =& \frac{2\lambda_{R_cE_k}}{W_3}e^{-\frac{\lambda_{R_cE_k}W_4}{W_3}}\sqrt{\frac{\beta_6}{\gamma_6}}K_1\left(2\sqrt{\beta_6\gamma_6}\right)\\
&-\frac{\lambda_{R_cE_k}}{W_3}e^{-\frac{\lambda_{R_cE_k}W_4}{W_3}}\frac{\pi u_6}{2Y_6}\sum_{l_6=0}^{Y_6}e^{-\frac{2\beta_6}{u_6\left(\delta_{l_6}+1\right)}-\frac{u_6\gamma_6\left(\delta_{l_6}+1\right)}{2}}\\
&\times\sqrt{1-\delta^2_{l_6}}-e^{-\lambda_{BR_c}E_2-\lambda_{R_cE_k}O_2},
\end{aligned} \tag{D.5}$$

$$Q_4 = e^{-\lambda_{R_cE_k}\Theta_6-\lambda_{BR_c}E_2}. \tag{D.6}$$

Let's substitute (D.5) and (D.6) into (D.4), (55) can be derived; set $\kappa_{R_cE_k}=0$ and $\sigma^2_{e_{R_cE_k}}=0$, we can derive the (56).

REFERENCES

[1] F. H. P. Fitzek and M. D. Katz, *Cooperation in Wireless Networks: Principles and Applications*. Dordrecht, The Netherlands: Springer, 2006.

[2] N. Kapucu, M. Bilim, and I. Develi, "A comprehensive performance analysis of relay-aided CDMA communications over dissimilar fading channels," *AEU-Int. J. Electron. Commun.*, vol. 83, pp. 339–347, Jan. 2018.

[3] N. Kapucu, M. Bilim, and I. Develi, "Average symbol error rate and outage probability of DS-CDMA systems with AF relaying over asymmetric fading channels," *Physical Commun.*, vol. 23, pp. 76–83, Jun. 2017.

[4] G. Altın, U. Aygolu, E. Başar, and M. E. Çelebi, "Outage probability analysis of cooperative spatial modulation systems," in *Proc. 23rd Int. Conf. Telecommun.*, May 2016, pp. 1–5.

[5] J. Li, X. Li, Y. Liu, C. Zhang, L. Li, and A. Nallanathan, "Joint impact of hardware impairments and imperfect channel state information on multi-relay networks," *IEEE Access*, vol. 7, pp. 72358–72375, 2019.

[6] X. Li, J. Li, and L. Li, "Performance analysis of impaired SWIPT NOMA relaying networks over imperfect weibull channels," *IEEE Syst. J.*, to be published.

[7] X. Chen, L. Guo, X. Li, C. Dong, J. Lin, and P. T. Mathiopoulos, "Secrecy rate optimization for cooperative cognitive radio networks aided by a wireless energy harvesting jammer," *IEEE Access*, vol. 6, pp. 34127–34134, Jun. 2018.

[8] A. D. Wyner, "The wire-tap channel," *Bell Syst. Tech. J.*, vol. 54, no. 8, pp. 1355–1387, 1975.

[9] P. Parada and R. Blahut, "Secrecy capacity of SIMO and slow fading channels," in *Proc. IEEE Int. Symp. Inf. Theory*, Adelaide, SA, Australia, Sep. 2005, pp. 2152–2155.

[10] S. Shafiee and S. Ulukus, "Achievable rates in Gaussian MISO channels with secrecy constraints," in *Proc. IEEE Int. Symp. Inf. Theory*, Nice, France, Jun. 2007, pp. 2466–2470.

[11] Q. Yang, H.-M. Wang, Y. Zhang, and Z. Han, "Physical layer security in MIMO backscatter wireless systems," *IEEE Trans. Wireless Commun.*, vol. 15, no. 11, pp. 7547–7560, Nov. 2016.

[12] W. Zeng, J. Zhang, S. Chen, K. P. Peppas, and B. Ai, "Physical layer security over fluctuating two-ray fading channels," *IEEE Trans. Veh. Technol.*, vol. 67, no. 9, pp. 8949–8953, Sep. 2018.

[13] J. N. Laneman, D. N. C. Tse, and G. W. Wornell, "Cooperative diversity in wireless networks: Efficient protocols and outage behavior," *IEEE Trans. Inf. Theory*, vol. 50, no. 12, pp. 3062–3080, Dec. 2004.

[14] X. Li, M. Matthaiou, Y. Liu, H. Q. Ngo, and L. Li, "Multi-pair two-way massive MIMO relaying with hardware impairments over Rician fading channels," in *Proc. IEEE GLOBECOM*, Abu Dhabi, UAE, Dec. 2018, pp. 1–6.

[15] X. Li, J. Li, Y. Liu, Z. Ding, and A. Nallanathan, "Outage performance of cooperative NOMA networks with hardware impairments," in *Proc. IEEE GLOBECOM*, Abu Dhabi, UAE, Dec. 2018, pp. 1–6.

[16] L. J. Rodriguez, N. H. Tran, T. Q. Duong, T. Le-Ngoc, M. Elkashlan, and S. Shetty, "Physical layer security in wireless cooperative relay networks: State of the art and beyond," *IEEE Commun. Mag.*, vol. 53, no. 12, pp. 32–39, Dec. 2015.

[17] L. Fan, X. Lei, N. Yang, T. Q. Duong, and G. K. Karagiannidis, "Secure multiple amplify-and-forward relaying with cochannel interference," *IEEE J. Sel. Topics Signal Process.*, vol. 10, no. 8, pp. 1494–1505, Dec. 2016.

[18] F. Yarkin, I. Altunbas, and E. Basar, "Source transmit antenna selection for space shift keying with cooperative relays," *IEEE Commun. Lett.*, vol. 21, no. 5, pp. 1211–1214, May 2017.

[19] N. Kapucu, M. Bilim, and I. Develi, "Outage performance of cooperative DS-CDMA systems with best path selection over $\alpha-\eta-\mu$ fading channels," *Electron. Lett.*, vol. 53, no. 11, pp. 752–754, May 2017.

[20] O. C. Öztoprak, F. Yarkin, I. Altunbas, and E. Basar, "Performance analysis of space shift keying for AF relaying with relay selection," *AEU-Int. J. Electron. Commun.*, vol. 81, pp. 74–82, Nov. 2017.

[21] Y. Zou, X. Wang, and W. Shen, "Optimal relay selection for physical-layer security in cooperative wireless networks," *IEEE J. Sel. Areas Commun.*, vol. 31, no. 10, pp. 2099–2111, Oct. 2013.

[22] S. Atapattu, N. Ross, Y. Jing, Y. He, and J. S. Evans, "Physical-layer security in full-duplex multi-hop multi-user wireless network with relay selection," *IEEE Trans. Wireless Commun.*, vol. 18, no. 2, pp. 1216–1232, Feb. 2019.

[23] L. Wang, N. Yang, M. Elkashlan, P. L. Yeoh, and J. Yuan, "Physical layer security of maximal ratio combining in two-wave with diffuse power fading channels," *IEEE Trans. Inf. Forensics Security*, vol. 9, no. 2, pp. 247–258, Feb. 2014.

[24] R. Tang, J. Cheng, and Z. Cao, "Contract-based incentive mechanism for cooperative NOMA systems," *IEEE Commun. Lett.*, vol. 23, no. 1, pp. 172–175, Jan. 2019.

[25] T. Kim and M. Dong, "An iterative Hungarian method to joint relay selection and resource allocation for D2D communications," *IEEE Wireless Commun. Lett.*, vol. 3, no. 6, pp. 625–628, Dec. 2014.

[26] R. Tang, J. Zhao, H. Qu, Z. Zhu, and Y. Zhang, "Joint mode selection and resource allocation for mobile relay-aided device-to-device communication," *KSII Trans. Int. Inf. Syst.*, vol. 10, no. 3, pp. 950–975, Mar. 2016.

[27] J. G. Proakis, *Digital Communications*. New York, NY, USA: McGraw-Hill, 1995.

[28] Y. Chen, "Energy-harvesting AF relaying in the presence of interference and Nakagami-*m* fading," *IEEE Trans. Wireless Commun.*, vol. 15, no. 2, pp. 1008–1017, Feb. 2016.

[29] A. Salem, K. A. Hamdi, and K. M. Rabie, "Physical layer security with RF energy harvesting in af multi-antenna relaying networks," *IEEE Trans. Commun.*, vol. 64, no. 7, pp. 3025–3038, Jul. 2016.

[30] K. M. Rabie, B. Adebisi, and M.-S. Alouini, "Half-duplex and full-duplex AF and DF relaying with energy-harvesting in log-normal fading," *IEEE Trans. Green Commun. Netw.*, vol. 1, no. 4, pp. 468–480, Dec. 2017.

[31] I. Krikidis, S. Timotheou, S. Nikolaou, G. Zheng, D. W. K. Ng, and R. Schober, "Simultaneous wireless information and power transfer in modern communication systems," *IEEE Commun. Mag.*, vol. 52, no. 11, pp. 104–110, Nov. 2014.

[32] H. Xing, K.-K. Wong, Z. Chu, and A. Nallanathan "To harvest and jam: A paradigm of self-sustaining friendly jammers for secure AF relaying," *IEEE Trans. signal Process.*, vol. 63, no. 24, pp. 6616–6631, Dec. 2015.

[33] E. Boshkovska, D. W. K. Ng, N. Zlatanov, A. Koelpin, and R. Schober, "Robust resource allocation for MIMO wireless powered communication networks based on a non-linear EH model," *IEEE Trans. Commun.*, vol. 65, no. 5, pp. 1984–1999, May 2017.

[34] Z. Ding, C. Zhong, D. W. K. Ng, M. Peng, H. A. Suraweera, R. Schober, and H. V. Poor, "Application of smart antenna technologies in simultaneous wireless information and power transfer," *IEEE Commun. Mag.*, vol. 53, no. 4, pp. 86–93, Apr. 2015.

[35] L. Jiang, H. Tian, Z. Xing, K. Wang, K. Zhang, S. Maharjan, S. Gjessing, and Y. Zhang, "Social-aware energy harvesting device-to-device communications in 5G networks," *IEEE Wireless Commun.*, vol. 23, no. 4, pp. 20–27, Aug. 2016.

[36] S. Bi, C. K. Ho, and R. Zhang, "Wireless powered communication: Opportunities and challenges," *IEEE Commun. Mag.*, vol. 53, no. 4, pp. 117–125, Apr. 2015.

[37] M. Babaei, U. Aygolu, and E. Basar, "Cooperative AF relaying with energy harvesting in Nakagami-*m* fading channel," *Phys. Commun.*, vol. 34, pp. 105–113, Jun. 2019.

[38] A. A. Nasir, X. Zhou, S. Durrani, and R. A. Kennedy, "Relaying protocols for wireless energy harvesting and information processing," *IEEE Trans. Wireless Commun.*, vol. 12, no. 7, pp. 3622–3636, Jul. 2013.

[39] Z. Mobini, M. Mohammadi, and C. Tellambura, "Wireless-powered full-duplex relay and friendly jamming for secure cooperative communications," *IEEE Trans. Inf. Forensics Security*, vol. 14, no. 3, pp. 621–634, Mar. 2019.

[40] J. Qiao, H. Zhang, X. Zhou, and D. Yuan, "Joint beamforming and time switching design for secrecy rate maximization in wireless-powered FD relay systems," *IEEE Trans. Veh. Technol.*, vol. 67, no. 1, pp. 567–579, Jan. 2018.

[41] A. Alsharoa, H. Ghazzai, A. E. Kamal, and A. Kadri, "Optimization of a power splitting protocol for two-way multiple energy harvesting relay system," *IEEE Trans. Green Commun. Netw.*, vol. 1, no. 4, pp. 444–457, Dec. 2017.

[42] H. Lee, C. Song, S.-H. Choi, and I. Lee, "Outage probability analysis and power splitter designs for SWIPT relaying systems with direct link," *IEEE Commun. Lett.*, vol. 21, no. 3, pp. 648–651, Mar. 2017.

[43] Y. Lou, Y. Zheng, J. Cheng, and H. Zhao, "Performance of SWIPT-based differential AF relaying over Nakagami- *m* fading channels with direct link," *IEEE Wireless Commun. Lett.*, vol. 7, no. 1, pp. 106–109, Feb. 2018.

[44] T. Schenk, *RF Imperfections in High-Rate Wireless Systems: Impact and Digital Compensation*. Amsterdam, The Netherlands: Springer, 2008.

[45] E. Björnson, J. Hoydis, M. Kountouris, and M. Debbah, "Massive MIMO systems with non-ideal hardware: Energy efficiency, estimation, and capacity limits," *IEEE Trans. Inf. Theory*, vol. 60, no. 11, pp. 7112–7139, Nov. 2014.

[46] E. Björnson, M. Matthaiou, and M. Debbah, "A new look at dual-hop relaying: Performance limits with hardware impairments," *IEEE Trans. Commun.*, vol. 61, no. 11, pp. 4512–4525, Nov. 2013.

[47] X. Li, M. Huang, X. Tian, H. Guo, J. Jin, and C. Zhang, "Impact of hardware impairments on large-scale MIMO systems over composite RG fading channels," *AEU-Int. J. Electron. Commun.*, vol. 88, pp. 134–140, May 2018.

[48] K. Ishibashi, C. K. Ho, and I. Krikidis, "Diversity-multiplexing tradeoff of dynamic harvest-and-forward cooperation," *IEEE Wireless Commun. Lett.*, vol. 4, no. 6, pp. 633–636, Dec. 2015.

[49] Y. Dong, M. J. Hossain, and J. Cheng, "Performance of wireless powered amplify and forward relaying over Nakagami-*m* fading channels with nonlinear energy harvester," *IEEE Commun. Lett.*, vol. 20, no. 4, pp. 672–675, Apr. 2016.

[50] L. Peng, G. Zang, Q. Zhou, Y. Gao, and C. Xi, "Security performance analysis for cooperative communication system under Nakagami-*m* fading channel," in *Proc. IEEE 17th Int. Conf. Commun. Technol. (ICCT)*, Oct. 2017, pp. 187–192.

[51] M. Babaei, U. Aygölü, and E. Basar, "BER analysis of dual-hop relaying with energy harvesting in Nakagami-*m* fading channel," *IEEE Trans. Wireless Commun.*, vol. 17, no. 7, pp. 4352–4361, Jul. 2018.

[52] Z. Chen, Z. Chi, Y. Li, and B. Vucetic, "Error performance of maximal-ratio combining with transmit antenna selection in flat Nakagami-*m* fading channels," *IEEE Trans. Wireless Commun.*, vol. 8, no. 1, pp. 424–431, Jan. 2009.

[53] I. S. Gradshteyn and I. M. Ryzhik, *Table of Integrals, Series, and Products*. New York, NY, USA: Academic, Sep. 2014.

[54] F. B. Hildebrand, *Introduction to Numerical Analysis*. North Chelmsford, MA, USA: Courier Corporation, 1987.

[55] J. Zhang, G. Pan, and Y. Xie, "Secrecy analysis of wireless-powered multi-antenna relaying system with nonlinear energy harvesters and imperfect CSI," *IEEE Trans. Green Commun. Netw.*, vol. 2, no. 2, pp. 460–470, Jun. 2018.

[56] M. Babaei, U. Aygolo, and L. D. Ata, "Performance of selective decode-and-forward SWIPT network in Nakagami-M fading channel," in *Proc. 26th Telecommun. Forum (TELFOR)*, Nov. 2018, pp. 1–4.

XINGWANG LI (S'14–M'15) received the B.Sc. degree in communication engineering from Henan Polytechnic University, China, in 2007, the M.Sc. degree from the National Key Laboratory of Science and Technology on Communications, University of Electronic Science and Technology of China (UESTC), in 2010, and the Ph.D. degrees in communication and information system from the State Key Laboratory of Networking and Switching Technology, Beijing University of Posts and Telecommunications (BUPT), in 2015. From 2010 to 2012, he was an Engineer with Comba Telecom Ltd., Guangzhou, China. From 2017 to 2018, he was a Visiting Scholar with the Institute of Electronics, Communications and Information Technology (ECIT), Queen's University Belfast (QUB), Belfast, U.K. He is currently an Associated Professor with the School of Physics and Electronic Information Engineering, Henan Polytechnic University, Jiaozuo, China. He has published several papers in journal and conferences, holds several patents, and has involved in several funded research projects on the wireless communications areas. His research interests include MIMO communication, cooperative communication, hardware constrained communication, NOMA, physical layer security, UAV, FSO communications, and performance analysis of fading channels. He has served a TPC member of IEEE Globecom Workshop 18'. He serves as a TPC member of IEEE/CIC ICCC workshop 19'. He currently serves as an Associate Editor of IEEE ACCESS and an Editor of the *KSII Transactions on Internet and Information Systems*.

MENGYAN HUANG (S'19) received the B.Sc. degree in communication engineering (wireless mobile communication direction) from the College of Electronic Information Engineering, Sias International College of Zhengzhou University, in 2017. She is currently pursuing the M.Sc. degree in communication and information systems with the School of Physics and Electronic Information Engineering, Henan Polytechnic University, Jiaozuo, China. Her current research interests include massive MIMO and physical layer secure communication.

CHANGSEN ZHANG received the Ph.D. degree from the China University of Mining and Technology, in 2003, and the B.S. degree from Northeast University, China, in 1992. He is currently a Full Professor and a Ph.D. Tutor of telecommunications with the Department of Communication and Information System, Henan Polytechnic University. He is an outstanding young science and technology expert in Jiaozuo and serves as an Academic Leader of information and communication engineering in Henan. His main research interests include wireless sensor networks, modern communications technology, and wireless networks' protocols. He was a recipient of Provincial Science and Technology Progress Award.

DAN DENG received the bachelor's and Ph.D. degrees from the Department of Electronic Engineering and Information Science, University of Science and Technology of China, in 2003 and 2008, respectively. From 2008 to 2014, he was the Director with Comba Telecom Ltd., Guangzhou, China. Since 2014, he has been with Guangzhou Panyu Polytechnic, where he is currently an Associate Professor. He has published 45 papers in international journals and conferences and holds 19 patents. His research interests include MIMO communication and physical-layer security in next-generation wireless communication systems. He has served as a member of Technical Program Committees for several conferences.

KHALED M. RABIE received the B.Sc. degree (Hons.) in electrical and electronic engineering from the University of Tripoli, Tripoli, Libya, in 2008, and the M.Sc. and Ph.D. degrees in communication engineering from The University of Manchester, Manchester, U.K., in 2010 and 2015, respectively. He is currently a Postdoctoral Research Associate with Manchester Metropolitan University (MMU), Manchester. His research interests include signal processing and the analysis of power line and wireless communication networks. He is a fellow of the U.K. Higher Education Academy. He was a recipient of the Best Student Paper Award at the IEEE ISPLC, TX, USA, in 2015, and the MMU Outstanding Knowledge Exchange Project Award, in 2016. He is currently the Program Chair of the IEEE ISPLC 2018, the Co-Chair of the IEEE CSNDSP 2018 Green Communications and Networks track, and the Publicity Chair of the INISCOM 2018. He is also an Associate Editor of IEEE Access and an Editor of the *Physical Communication* journal (Elsevier).

YUAN DING received the bachelor's degree from Beihang University (BUAA), Beijing, China, in 2004, the master's degree from Tsinghua University, Beijing, in 2007, and the Ph.D. degree from Queen's University of Belfast, Belfast, U.K., in 2014, all in electronic engineering. He was a Radio Frequency (RF) Engineer in Motorola R&D Centre, Beijing, from 2007 to 2009. He was an RF Field Application Engineer with Freescale Semiconductor Inc., Beijing, from 2009 to 2011, responsible for high power base-station amplifier design. He is currently an Assistant Professor with the Institute of Sensors, Signals and Systems (ISSS), Heriot-Watt University, Edinburgh, U.K. His research interests include antenna array, physical layer security, and 5G related areas. He was a recipient of the IET Best Student Paper Award at LAPC 2013 and the Young Scientists Awards in General Assembly and Scientific Symposium (GASS), 2014 XXXIst URSI.

JIANHE DU received the B.Sc. and M.Sc. degrees from Yunnan University, Yunnan, China, in 2007 and 2010, respectively, and the Ph.D. degree from the Beijing University of Posts and Telecommunications, Beijing, China, in 2015. He is currently a Lecturer with the School of Information and Engineering, Communication University of China, Beijing. His research interests mainly include channel estimation, symbol detection, multiple-antenna systems, MIMO relay systems, and tensor-based signal processing applied to wireless communication. He was a Guest Editor for the Special Issue Applications of Tensor Models in Wireless Communications and Mobile Computing of the *Wireless Communications and Mobile Computing* journal.